AD 295 129

63-2-3

RADC-TDR-62-597

FINAL TECHNICAL REPORT

BEAM-TYPE PARAMETRIC AMPLIFIER

Covering the Period
19 January 1961 through 19 October 1962

ELECTRONIC TUBE DIVISION
SPERRY GYROSCOPE COMPANY
Division of Sperry Rand Corporation
GREAT NECK, NEW YORK

Contract No. AF30(602)-2433

Prepared for

ROME AIR DEVELOPMENT CENTER
AIR FORCE SYSTEMS COMMAND
UNITED STATES AIR FORCE
GRIFFISS AIR FORCE BASE
NEW YORK

SPERRY REPORT NO. NA-8210-8333

NOVEMBER 1962

RADC-TDR-62-597

COPY NO. 1

FINAL TECHNICAL REPORT

BEAM-TYPE PARAMETRIC AMPLIFIER

Covering the Period
19 January 1961 through 19 October 1962

ELECTRONIC TUBE DIVISION
SPERRY GYROSCOPE COMPANY
Division of Sperry Rand Corporation
GREAT NECK, NEW YORK

Contract No. AF30(602)-2433
Project No. 5573 Task No. 55011

Prepared for

ROME AIR DEVELOPMENT CENTER
AIR FORCE SYSTEMS COMMAND
UNITED STATES AIR FORCE
GRIFFISS AIR FORCE BASE
NEW YORK

Prepared by
ENGINEERING DEPARTMENT
R. Eng
I. Itzkan
PUBLICATIONS DEPARTMENT
A. S. Ferello

SPERRY REPORT NO. NA-8210-8333

NOVEMBER 1962

FOREWORD

This final technical report, covering the period from 19 January 1961 through 19 October 1962, describes the beam-type parametric amplifier study conducted for the Rome Air Development Center of the U.S. Air Force Systems Command. The program was performed by the Electronic Tube Division, Sperry Gyroscope Company Division of Sperry Rand Corporation, Great Neck, New York under Contract No. AF30(602)-2433.

The authors wish to extend their most sincere thanks to the following individuals whose valuable contributions during the course of the program was greatly appreciated.

Dr. C.C. Wang

Dr. L. Holmboe

Dr. P. McIsaac

Dr. G. White

Mr. J. Litton

Mr. J. Herman

Mr. I. Abramowitz

Mr. W. Gehlich

Mr. A. Guarella

ABSTRACT

The objectives of the program are to demonstrate the feasibility of two beam-type parametric amplifiers, one capable of narrowband voltage-tuned operation, and the other capable of broadband untuned operation. The final technical report covers the theoretical and experimental studies of the characteristics of the fast cyclotron wave, coupler and pump circuits for the coupling and amplification of the cyclotron wave. Cold test data show that a chosen coupler is capable of operating over a 25-percent bandwidth provided a modification of the coupler interaction impedance is made. A Kompfner dip as high as 28 db has been observed in an experimental setup. An electronic gain of approximately 10 db has been obtained with a resonant pump operated at about 8 watts. The electron gun is a convergent-flow Pierce type. The effect of the magnetic flux threading the cathode is discussed. Voltage-tuned operations are discussed, and a design for an X-band fixed-tuned broadband degenerate device is given.

Recommendations are made for future study of devices of this type.

TABLE OF CONTENTS

Section		Page
I	INTRODUCTION	1
II	DISCUSSION	3
	2-1. General Theory	3
	2-2. Coupler Circuits	11
	2-3. Kompfner-Dip Experiment	18
	2-4. Signal Attenuation Experiments	23
	2-5. Oscillation	26
	2-6. Coupling Between Bifilar Helix Coupler and External Circuit, and Cold Circuit Loss	26
	2-7. Pump Circuit	30
	2-8. Degenerate Device Operation	36
	2-9. Voltage-Tuned Operation	41
	2-10. An X-Band Design of a Fixed-Tuned Broadband Degenerate Device	43
III	CONCLUSIONS	47
IV	RECOMMENDATIONS	49
	REFERENCES	51
	BIBLIOGRAPHY	53

LIST OF ILLUSTRATIONS

Figure		Page
1	Essential Components of a Beam-Type Parametric Amplifier	4
2	Fast Cyclotron Wave ω-β Characteristics	4
3	Two Helices, One-Half Cyclotron Wavelength Displaced	13
4	Elliptical Helix Coupler, Cross-Sectional View	13
5	ω-β Characteristics of Coupled Elliptic Helices Spaced 1/2-Inch Apart	13
6	Transverse Impedance of Coupled Elliptic Helices Spaced 1/2-Inch Apart (Transverse Bead Size 1/4-Inch)	14
7	Typical Zig-Zag Line	14
8	ω-β Characteristics of Coupled Zig-Zag Lines P = 0.320 Inch, Line Width = 2 Inches, Spacing Between Lines = 0.025 Inch	15
9	Transverse Impedance of Coupled Zig-Zag Lines Spaced 1/4-Inch Apart, Beam Size 1/16-Inch Diameter Placed Equal Distance From Lines	16
10	Representative Modified Bifilar Helix	16
11	ω-β Characteristics of the Modified Bifilar Helix Coupler - 0.150-Inch Spacing	17
12	ω-β Characteristics of the Modified Bifilar Helix Coupler - 0.075-Inch Spacing	17

LIST OF ILLUSTRATIONS (CONT)

Figure		Page
13	Transverse Impedance of Modified Bifilar Helix	19
14	Kompfner Dip Experimental Apparatus	20
15	Axial Magnetic Field Versus Distance	20
16	Kompfner Dip Experimental Measurement	22
17	ω-β Characteristics of a Modified Bifilar Helix	22
18	Kompfner Dip Versus Normalized Beam Current	24
19	Kompfner Dip Versus Frequency	25
20	Velocity Spread Experimental Apparatus	25
21	Cathode Flux Linkage Versus Cathode Magnet Current	27
22	Signal Loss on Beam Versus Auxiliary Magnet Current	27
23	Method of Coupling to the Anti-Symmetrical Mode of a Bifilar Helix	28
24	Current Phase of the Out-of-Phase Mode of a Bifilar Helix	28
25	VSWR for Improved Method of Matching and Cold Loss Rate of Modified Bifilar Helix	29
26	TE_{11} Square Waveguide Loaded with Quadrupolar Elements	31
27	Four-Bar Quadrupole Circuit	32
28	ω-β Characteristics of Four-Bar Quadrupole Circuit P = 0.120 Inch	33
29	ω-β Characteristics of Four-Bar Quadrupole Circuit P = 0.060 Inch	34
30	Impedance of Four-Bar Quadrupole Circuit P = 0.120 Inch	35

LIST OF ILLUSTRATIONS (CONT)

Figure		Page
31	Field Pattern Half-Way Between Posts of Pump Circuit at 4775 Mc	37
32	ω-β Measurement Equipment	38
33	ω-β Characteristics of a Quadrifilar Helix	39
34	Modified Quadrifilar Helix	39
35	Experimental Setup for Measuring Electronic Gain	40
36	Scope Trace of Output Signal Level	40
37	Electronic Gain Versus Frequency	42
38	Electronic Gain Versus Pump Power	42
39	Electronic Gain Versus Input Signal	42
40	Fixed Pump Point, Variable Uniform Magnetic Field and Variable Uniform Beam Voltage Operation	44
41	Fixed Uniform Magnetic Field, Variable Pump Point and Variable Uniform Beam Voltage Operation	44
42	Fixed Pump Point, Fixed Uniform Magnetic Field and Variable Coupler Voltage Operation	45
43	Fixed Pump Point, Fixed Uniform Beam Voltage and Variable Coupler Magnetic Field Operation	45

SECTION I

INTRODUCTION

The purpose of this program was to demonstrate the feasibility of two beam-type parametric amplifiers; one capable of narrowband voltage-tuned operation and the other capable of broadband untuned operation. Parametric amplifiers having the following characteristics are objectives of the study:

- Operating Range
  - (1) Voltage-tuned operation over the frequency range of 7.5 to 12.5 Gc at rates up to 10^5 cps
  - (2) Untuned operation over the frequency range of 7.5 to 12.5 Gc
- 25-db minimum gain; total gain variation less than 6 db over the frequency range
- 3-db instantaneous bandwidth of 20 ± 5 mc for voltage-tuned operation; 5 Gc bandwidth for untuned operation
- 1-db maximum over-all amplifier single-channel noise figure
- 1-milliwatt minimum power output
- High operational stability and reverse attenuation, large dynamic range, minimum spurious responses
- Acceptance of pulse and continuous-wave signals
- 50-ohm nominal input and output impedance
- Compact size and weight, and low pump-power requirements
- 1500-hour minimum service life.

Feasibility studies were conducted at approximately:

$$f_{pump} = 6.0 \text{ Gc}$$

$$f_{signal} = 3.00 \pm 0.25 \text{ Gc}$$

$$f_{idler} = 3.00 \pm 0.25 \text{ Gc}$$

The beam-type parametric amplifier consists of a low-noise gun, followed by a signal-frequency coupler. This coupler introduces the signal to the beam in the form of a fast cyclotron wave, and removes noise from the beam at the signal

frequency. Following this signal-frequency coupler may be an idler coupler which removes beam noise at the idler frequency. Next, a pump circuit provides gain for both signal and idler frequencies. An output signal coupler extracts the amplified fast cyclotron wave from the beam. A collector then absorbs the d-c beam and the idler modulation. The entire device is immersed in an axially directed magnetic field.

SECTION II

DISCUSSION

2-1. GENERAL THEORY

Recent interest in the electron-beam parametric amplifier stems from the fact that in this type of device the noise contribution from the electron beam can theoretically be reduced to zero. Theoretically this is possible because of the positiveness of the kinetic power of the noise propagating on the beam as a fast cyclotron wave. The process of noise minimization is quite different from that in low-noise traveling-wave tubes which depends on the correlations of the beam current fluctuation and the velocity fluctuation.

Figure 1 shows the essential components of a beam-type parametric amplifier. For broadband untuned operation, it shows that the device consists of an input coupler, a pump and an output coupler, and an electron beam passing through all of the circuit components. At the input coupler, a signal at frequency ω_s is introduced and is transferred to the beam. The beam noise at ω_s, which propagates on the beam in the form of a fast cyclotron wave, is removed by the input coupler. The signal in the form of a fast cyclotron wave is then amplified in the pump region by the action of the pump field maintained by the pump source at pump frequency ω_p. In the amplification process, an idler signal at frequency ω_i is generated just as in any other parametric device. The amplified signal is then coupled out to the circuit by the output coupler. To meet the objectives of the program, the following general considerations are discussed:

A. Circuit Parameters

The signal and idler wave propagation on the beam is in the form of a fast cyclotron wave, which has an exponential dependence

$$e^{j(\omega_s t - \beta_s z - \phi)}$$

and

$$e^{j(\omega_i t - \beta_i z - \phi)}$$

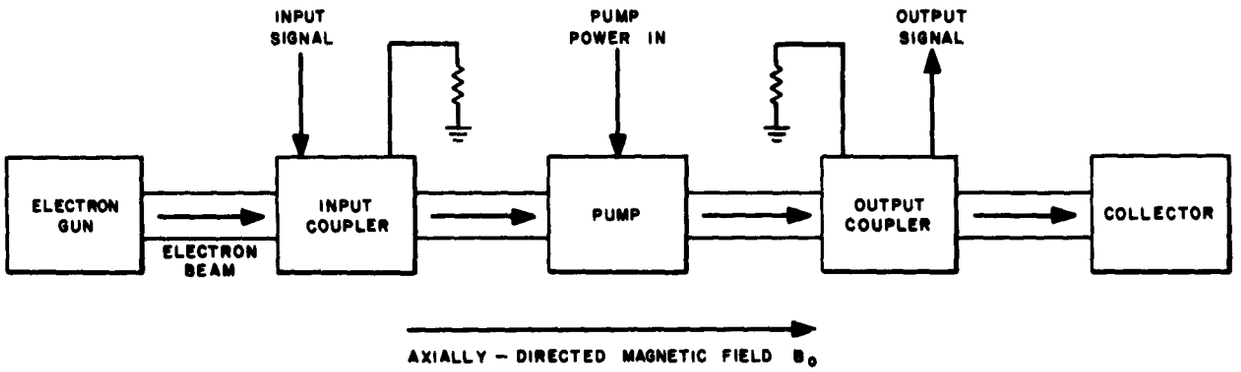

FIGURE 1. ESSENTIAL COMPONENTS OF A BEAM-TYPE PARAMETRIC AMPLIFIER

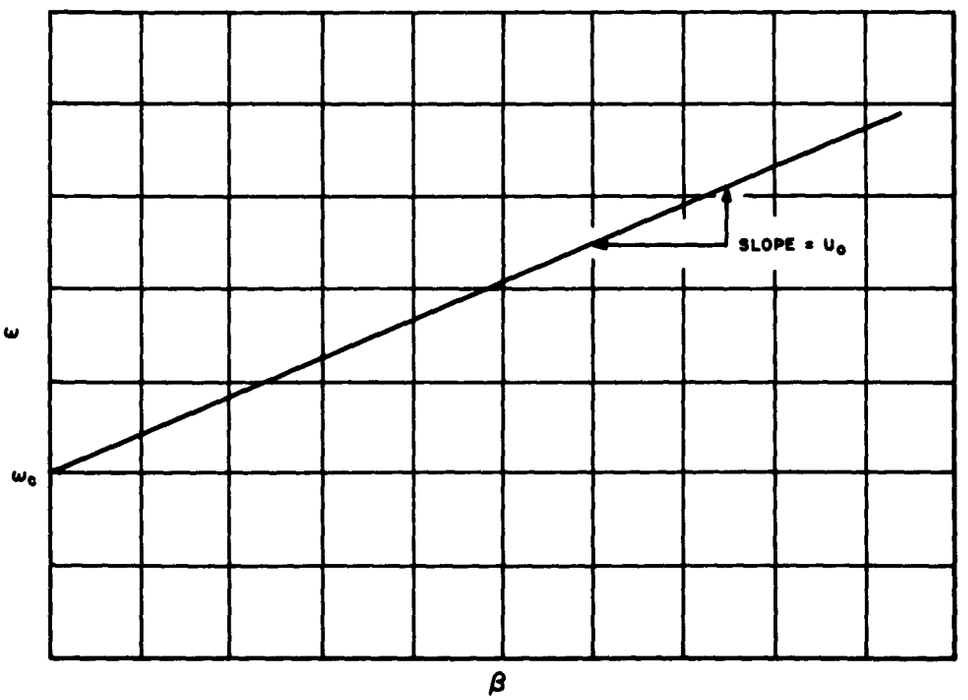

FIGURE 2. FAST CYCLOTRON WAVE ω-β CHARACTERISTICS

where z, t, ϕ denote respectively the axial distance, time, and angular coordinate and ω, β without the subscripts denote radian frequency and propagation constant. For a given axial electron velocity u_o, and a given cyclotron frequency ω_c or magnetic field B_o, the fast cyclotron wave has an $\omega - \beta$ relation characterized by the equation

$$\omega = u_o \beta + \omega_c = u_o \beta + \eta B_o \tag{1}$$

where η is the charge-to-mass ratio of an electron at rest.

Equation (1) is linear in the $\omega - \beta$ plane and is plotted in figure 2. The slope of the line is the group velocity of the wave and it is equal to u_o. The ω-axis intercept is ω_c. In order to excite this wave on the beam efficiently, a circuit must support a wave that is synchronous to the fast cyclotron wave. In particular, for broadband untuned operation in which both the voltage and magnetic field are fixed, the group velocity of the circuit wave must be equal to the beam velocity in the signal frequency range of interest. Another point of importance is that the fast cyclotron wave involves only the transverse motion of the electron beam. Since the main driving force at low-beam velocity is the Coulomb force, only the transverse electric field of the circuit is involved in the interaction equation. The remaining coupler circuit parameter is the Kompfner-dip length which is given by the equation:

$$L_k = \frac{\lambda_g}{2} \sqrt{\frac{2V_o}{I_o} \frac{\omega_c}{\omega_s} \frac{1}{K_t}} \tag{2}$$

where

L_k = Coupler length in meters

λ_g = Guide wavelength in meters

V_o = Beam voltage in volts

I_o = Beam current in amperes

ω_c = Radian cyclotron frequency

ω_s = Radian signal frequency

K_t = Transverse Pierce impedance for the circularly polarized wave in ohms.

Complete noise stripping requires that the exact Kompfner-dip length be used.

Next, consider the requirements of the pump circuit which functions as the coupling element between the signal and idler wave on the beam. For efficient coupling, the circuit pump wave must be of the form

$$e^{j(\omega_i + \omega_s)t - j(\beta_s + \beta_i)z - j2\phi}$$

Letting

$$\omega_i + \omega_s = \omega_p$$

$$\beta_i + \beta_s = \beta_p$$

it is possible to design a circuit to have this characteristic. For ease of operation as well as constant electronic gain, it is desirable to keep the pump frequency and propagation constant β fixed. This will be called fixed-pump operation. For fixed-pump operation, two methods of exciting the pump are possible. The pump can be operated as a resonant cavity or as a traveling-wave circuit. The electronic gain for these two types of operations are given by the following formulae:

$$G = 20 \log_{10} \cosh \frac{L}{B_o u_o r_o} \sqrt{2P Z_p(r_o) \beta^2} \quad \text{db} \tag{3}$$

$$G = 20 \log_{10} \cosh \frac{1}{B_o u_o r_o} \sqrt{P_o Z_p(r_o) Q_o \beta L \frac{v_g}{v_p}} \quad \text{db} \tag{4}$$

for nonresonant and resonant pumps, respectively.

where

G = Gain in db

L = Pump length in meter

B_o = Magnetic field in webers/square meter

u_o = Beam velocity in meters/second

r_o = Beam radius in meters

P = R-f power input to pump in watts

$Z_p(r_o)$ = Pierce impedance at r_o for the circularly polarized pump wave

β = Pump propagation constant

v_g = Group velocity at the pump point

v_p = Phase velocity at the pump point

Q_o = Unloaded Q of the cavity

P_o = Power loss in the cavity in watts

P = Power to traveling wave in watts.

It is interesting to note that the gain is proportional to the pump length for the nonresonant case, and to the square root of the pump length for the resonant case. At a high value of Q, the pump length for the resonant case is shorter and this advantage can be utilized in the pump design.

The general requirements to be satisfied by the output coupler are exactly the same as the input coupler. For sufficient r-f gain, however, the design is much less critical.

B. Beam Parameters

The electron beam parameters are the beam velocity u_o, beam radius r_o, and beam current I_o. A large range of values can be chosen provided the cathode current density for a given beam convergence does not exceed the maximum limit, and that the chosen Brillouin field is smaller than the cyclotron field. In addition, for a solid beam the beam perveance is a limiting factor; the highest solid beam perveance considered practical for this application is about 2×10^{-6}.

C. Noise Factor

When all the general requirements of the coupler circuit, pump circuit, and electron beam are met, successful operations of the device as an amplifier can be expected. To achieve very low-noise operation, however, a more detailed study of the loss parameters must be made. If a signal flow graph is made, it can be readily seen: (1) in order to preserve the input signal strength, the coupling loss caused by the mismatch between the external circuit and the input to the coupler circuit must be made small, (2) the coupler circuit cold loss must be small, (3) the Kompfner-dip length must be independent of frequency, and (4) the total cyclotron wave loss for a Kompfner-dip length must be small. The first three of these requirements are directly related to cold-circuit design and are more commonly known. The fourth requirement is discussed in detail in the following paragraphs:

A cyclotron wave may be thought of as a helical pattern of electrons which moves in the axial direction with nearly the beam velocity u_o. The separation between crests of the pattern is the cyclotron wavelength. Any axial motion of electrons in one part of the pattern relative to another part will tend to destroy the pattern and hence the signal.

Another way to visualize the situation is to realize that the locus of electrons of a particular phase is a helix. The locus of electrons which differ in phase from the first group by π radians is another helix which is axially displaced from the first by one-half cyclotron wavelength. (See figure 3.)

If a zero phase electron has an axial velocity which is slightly higher than the velocity of the π phase electron, it will begin to overtake the π phase electron. The time it takes the zero-phase electron to catch up depends on the difference in velocities and the relative distance (cyclotron wavelength). If this time is comparable to the transit time of the electrons through the circuit, the zero phase electron and the π phase electron will arrive at the same axial position at the exit plane of the circuit and will interfere destructively, completely nulling the signal.

There are three major sources of variation in axial velocity, which can result in cyclotron wave attenuation:

- Thermal velocities
- Potential variations caused by the space charge
- Potential variations caused by the electric and magnetic lenses.

The effects of these velocity variations are discussed individually.

If the overall length of the circuit is L, then the transit time through the circuit is $\tau = L/Z_o$ which to a first approximation is very nearly (L/u_o).

If the small differential in velocity, or error velocity is v_e, and the cyclotron wavelength is λ, then the time it would require v_e to transport an electron a distance $\lambda/2$ is τ_e, which is given by $\tau_e = \lambda/2v_e$.

If τ_e is equal to τ then during the transit through the circuit a zero phase electron will overtake a π phase electron, and the signal will be completely destroyed. Therefore, τ must be restricted to a small fraction of τ_e.

The difference in phase shift ϕ between the overtaken and overtaking electrons after they have traveled through a circuit of length L is given by

$$\phi = 2\pi \frac{v_e}{u_o} \frac{L}{\lambda}$$

and to preserve the signal, a requirement of ϕ_e is that it be a small fraction of a radian.

As the beam travels down the circuit, signal energy is coupled from the circuit to the beam and noise energy from the beam to the circuit. The length required for complete interchange of energy is called the Kompfner dip length, and a signal coupler must be one Kompfner dip length long. The Kompfner dip length for a circularly polarized wave is given by equation (2).

In order to replace the error velocity with an error potential let

$$\frac{1}{2}mv^2 = eV; \quad \frac{dV}{V} = \frac{2v\,dv}{v^2} = 2\frac{dv}{v}$$

or

$$\frac{v_e}{u_o} = \frac{1}{2}\frac{V_e}{V_o}$$

The phase shift becomes

$$\phi = \frac{\pi}{2}\left[\frac{V_e}{V_o}\right]\sqrt{\frac{\omega_c}{\omega}\left[\frac{V_o}{I_o K_t}\right]} = \frac{\pi}{2}\sqrt{\frac{\omega_c}{\omega}\left[\frac{V_e}{I_o K_t}\right]\frac{V_e}{V_o}}$$

1. Thermal Velocities

Suppose v_e is due only to thermal velocities. The emission from a cathode is half-Maxwellian in the axial direction. At 1200 °K this corresponds to about 0.2 volt. Using typical values of $\omega_c = \omega$, $V_o = 400v$, $I_o = 5$ ma, and $K_t = 250\ \Omega$ yields

$$\phi = \frac{\pi}{200}$$

for the thermal phase shift per coupler. This is a negligible amount.

2. Space Charge Potential Depression

The difference in potential between the beam edge and center of an immersed flow beam caused by the space charge is given to a first approximation by

$$V_e = V_o\ (0.015)K; \quad K = \text{microperveance.}$$

This causes the inside of the beam to move more slowly than the outside of the beam. The difference in phase between the inside and outside of the beam is, using

$$I_o = K\ V_o^{3/2} \times 10^{-6}$$

$$\phi = \frac{15\pi}{2}\sqrt{\frac{\omega_c}{\omega}\frac{K}{\sqrt{V_o K_t}}}$$

Using typical values of $\omega_c = \omega$, $V_o = 400v$, $I_o = 5$ ma, $K_t = 250\ \Omega$, and $K = 0.6$ yields

$$\phi = \frac{\pi}{10.}$$

To determine if this is a significant power loss, consider the fact that there is more current at the edge of the beam than in the center, and weigh the phases accordingly.

The variations in voltage across the beam are

$$V(r) = V_o\left[1 + 0.015\ K\left[\frac{r}{a}\right]^2\right]$$

Therefore, the variations in phase across the beam are

$$\phi = \phi_o \left[\frac{r}{a}\right]^2$$

where

$$\phi_o = \frac{15\pi}{2}\sqrt{\frac{\omega_c}{\omega}\left[\frac{K}{\sqrt{V_o K_t}}\right]}$$

The current between r and r + dr is $I = 2\pi r \rho\, dr$ where

$$\rho = \text{current density.}$$

The relative signal loss is then

$$\psi = \frac{\int_o^a I \cos\phi\, dr}{\int_o^a I\, dr} = \frac{\int_o^a 2\,\bar{a}\,\rho\, r \cos\left[\phi_o \frac{r^2}{a^2}\right] dr}{\int_o^a 2\pi r \rho\, dr} = -\frac{\text{Sin}\,\phi_o}{\phi_o}$$

and the power variations are

$$\psi^2 = \frac{\text{Sin}^2\,\phi_o}{\phi_o{}^2}$$

For $\phi_o = \pi/10$ the power is down by three-percent at the end of the coupler.

3. Lens Effects

At the present time, no good basis has been established for estimating the order of magnitude of the velocity variations caused by the electrostatic and magnetic lens effect introduced in the gun and focusing systems.

Gorden[1] estimates these effects to be ten times the space charge spread. If this figure is used it gives a phase spread of $\phi_o = \pi$ which attenuates the signal.

At any rate, both space charge and lens effect problems are minimized if Brillouin flow (no flux linking cathode) is used. In this case, when the uniform field region is reached the axial electron velocity is a constant for all electrons if beam entrance conditions have been successfully matched[2].

Therefore, Brillouin flow seems to be the best first choice for an experimental device.

Assuming a correct Kompfner dip length, a perfect r-f match and a zero beam wave attenuation constant, the noise factor of a beam-type parametric amplifier can be expressed by the equation

$$N F = 1 + \frac{Tc}{To}\left[e^{\frac{D}{8.68}} - 1 \right]$$

where

N F = Noise factor of the device

To = Input terminal temperature in °K

Tc = Coupler temperature in °K

D = Total coupler cold loss in db.

If the noise factor is expressed in db and Tc = To, the value of noise factor is exactly D/Z. Needless to say, it is very important to keep the value of D small. There are other means by which the signal can be degraded, but they are to be discussed when actual circuits are considered.

2-2. COUPLER CIRCUITS

Couplers whose function were to first introduce the signal onto the beam and then remove the amplified signal from the beam, were studied. Three types of circuits for use as a possible coupler were studied. The three types studied were:

- Coupled elliptic helix coupler
- Coupled zig-zag line coupler
- Modified bifilar helix coupler.

A. Coupled Elliptic Helix Coupler

A coupler circuit previously employed in a Sperry-sponsored research program was a flattened helix above a ground plane. This circuit was used above a ground plane because two such circuits, one above the other, do not remain balanced unless their uncoupled phase velocities are equal. It is difficult to fabricate this flattened helix circuit with sufficient repeatability to ensure the equality of the uncoupled phase velocities. An improved method of fabricating this circuit, using elliptical mandrels was employed. The resulting new coupler is called the coupled elliptic helix coupler. The circuit is supported as shown in figure 4. Dielectric loading and the turn-to-turn spacing were more easily controlled with this configuration. Cold test results of the coupled elliptic

helices propagation characteristics are shown on figure 5, and the transverse Pierce impedance of the transverse mode is shown on figure 6. The two helices have windings that are opposite in direction. The longitudinal mode was also measured at this time but was not plotted. The two modes are quite close when plotted on the $\omega - \beta$ plane. The group velocity of transverse mode is about one-eighth the velocity of the light. For broadband untuned operation, this will correspond to few thousand volts of beam voltage. The ratio of the cyclotron frequency to signal frequency is about one to four for broadband operation. In the impedance measurement, the spacing between the helices was made equal to twice the transverse bead length. The transverse bead was designed to perturb the transverse electric field only. Using the impedance and propagation data, a Kompfner-dip length was calculated to be several inches long for a reasonable value of beam current. The test structure was supported by several small diameter ceramic rods. The structure has a major axis equal to about one-half inch, and a minor axis equal to about one-eighth inch. When scaled to 10 Gc, the construction problem for an elliptic helix is severe, if not impossible. After initial study on this circuit attention was shifted to a more favorable circuit, the modified bifilar helix.

B. Coupled Zig-Zag Line Coupler

While the coupled elliptic helix coupler was being studied, there was a need for a dispersive coupler for a voltage-tuned operation. A zig-zag line appears to be quite promising as a coupling structure from the view point of high transverse interaction impedance and low phase velocity, in addition to the ease with which the dispersion characteristics can be altered. A typical zig-zag line is shown on figure 7. Using two coupled lines, one above the other, a coupled system was formed. In figure 8 and figure 9 plots of the propagation constants and transverse impedance of the coupled zig-zag lines are shown. The circuit is more dispersive than the coupled elliptic helix but the impedance is much lower. Because of the low-transverse impedance, the circuit is not suitable as a coupler.

C. Modified Bifilar Helix Coupler

This circuit was used in all of the hot tests in this program, i.e., tests in the presence of an interacting electron beam. A typical modified bifilar helix structure is shown on figure 10. As stated in the general theory discussion, a good coupler must have a high impedance so that signal degradation can be kept to a low value before amplification. In addition, there are other problems such as mode separation and mechanical support. A modified bifilar helix, such as the one shown in figure 10, has a very high transverse impedance. Further, the mechanical support problems, and the mode separation problems are much easier for the modified bifilar helix. Figures 11 and 12 show the $\omega - \beta$ characteristics of the modified bifilar helix, and represent the propagation characteristics of the transverse mode only. Since the $\omega - \beta$ characteristics of a regular bifilar helix is known, it was found that the modified bifilar helix has nearly the same propagation characteristics as that predicted for a regular bifilar helix. This is a distinct advantage because the result of any change in circuit parameter can be predicted accurately.

The operating value of ka for the modified bifilar helix is slightly greater than one. This fact represents the ease with which the circuit can be supported even at X-band. The actual fabrication of the circuit is not simple,

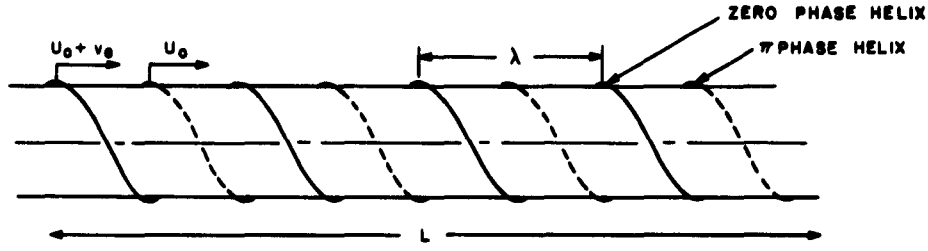

FIGURE 3. TWO HELICES, ONE-HALF CYCLOTRON WAVELENGTH DISPLACED

FIGURE 4. ELLIPTICAL HELIX COUPLER, CROSS-SECTIONAL VIEW

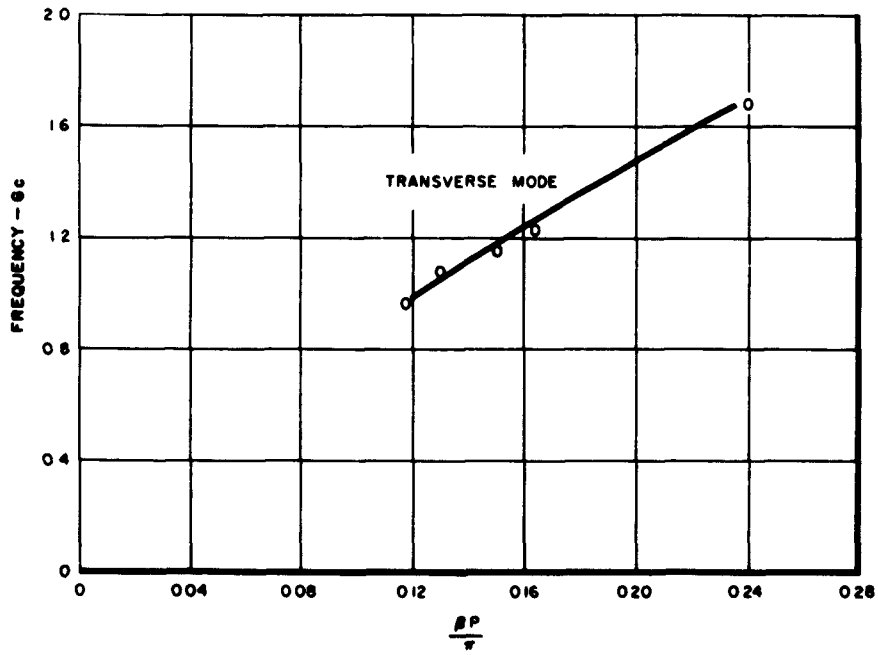

FIGURE 5. ω-β CHARACTERISTICS OF COUPLED ELLIPTIC HELICES SPACED 1/2-INCH APART

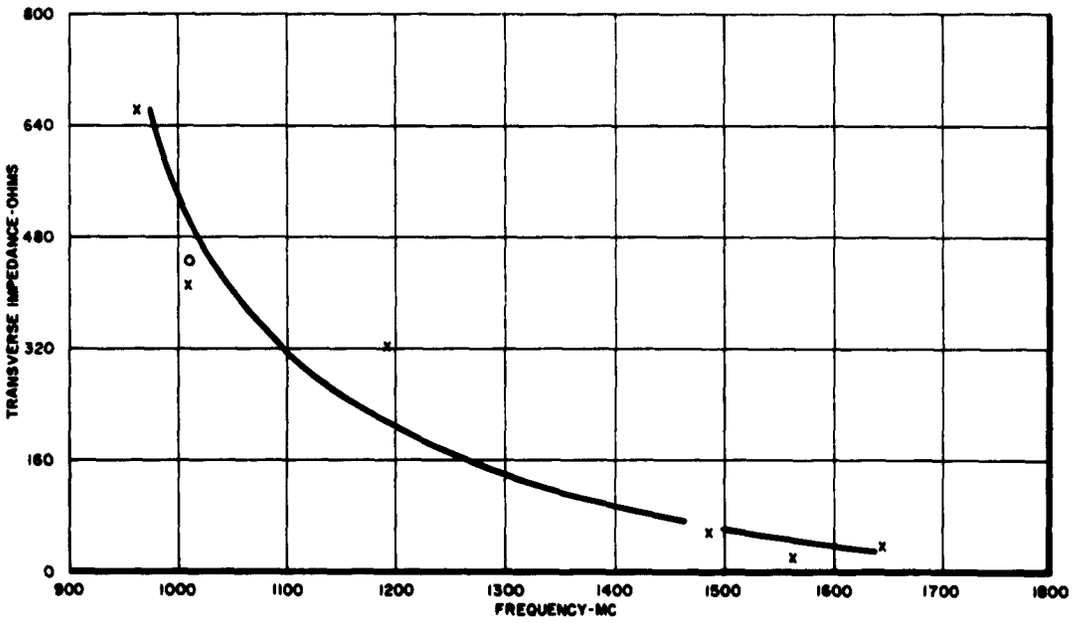

FIGURE 6. TRANSVERSE IMPEDANCE OF COUPLED ELLIPTIC HELICES SPACED 1/2-INCH APART (TRANSVERSE BEAD SIZE 1/4-INCH)

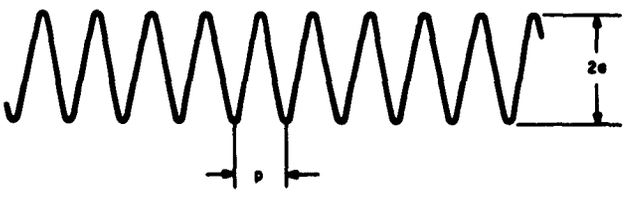

FIGURE 7. TYPICAL ZIG-ZAG LINE

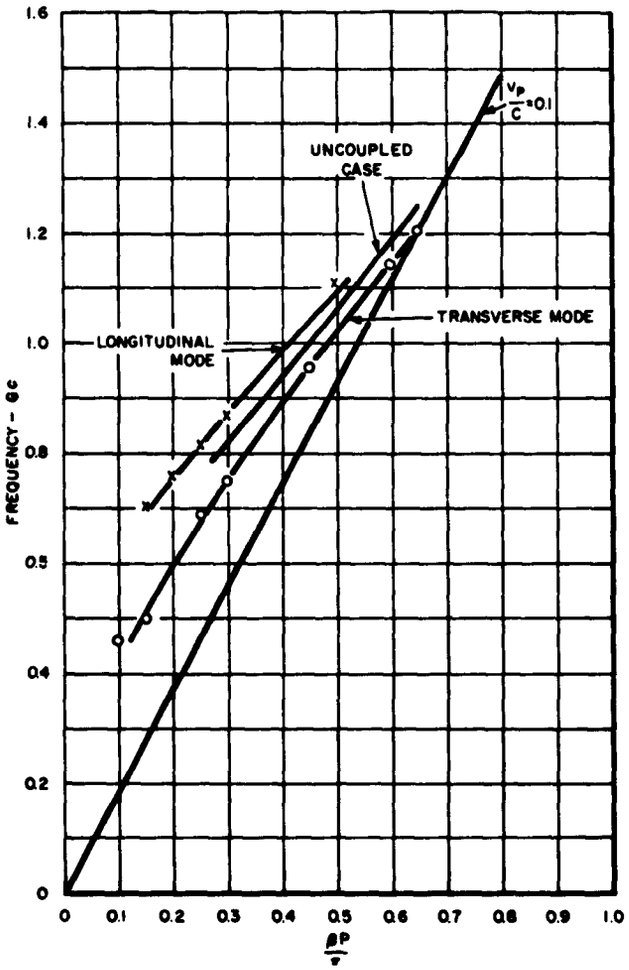

FIGURE 8. ω-β CHARACTERISTICS OF COUPLED ZIG-ZAG LINES P = 0.320 INCH, LINE WIDTH = 2 INCHES, SPACING BETWEEN LINES = 0.025 INCH

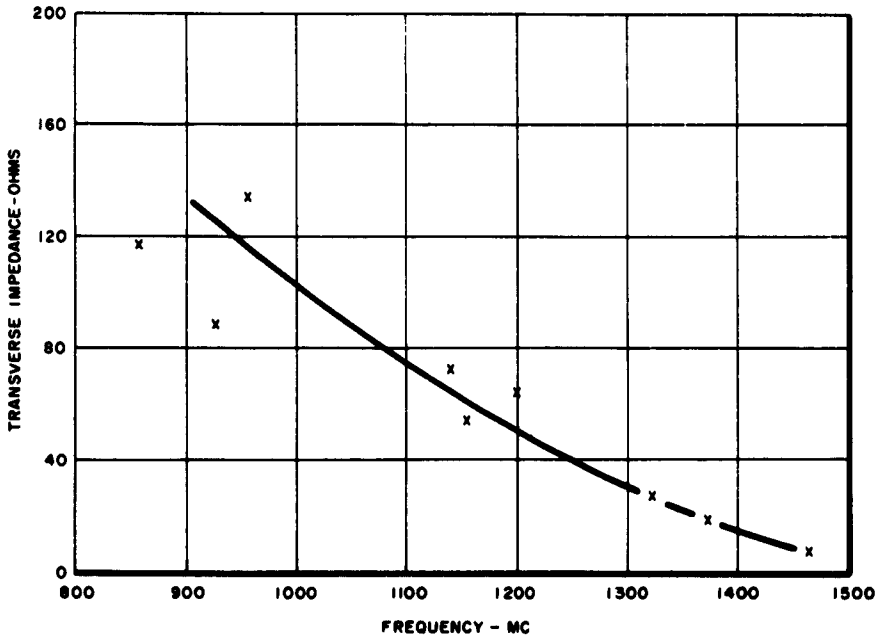

FIGURE 9. TRANSVERSE IMPEDANCE OF COUPLED ZIG-ZAG LINES SPACED 1/4-INCH APART, BEAM SIZE 1/16-INCH DIAMETER PLACED EQUAL DISTANCE FROM LINES

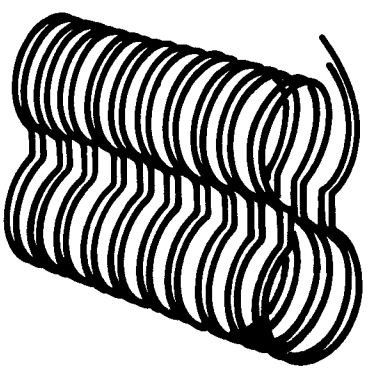

FIGURE 10. REPRESENTATIVE MODIFIED BIFILAR HELIX

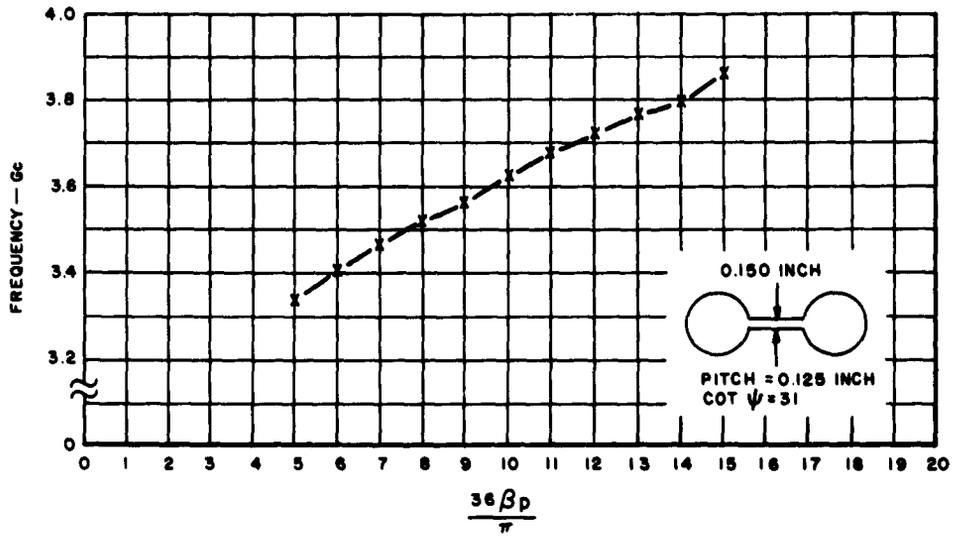

FIGURE 11. ω-β CHARACTERISTICS OF THE MODIFIED BIFILAR HELIX COUPLER - 0.150-INCH SPACING

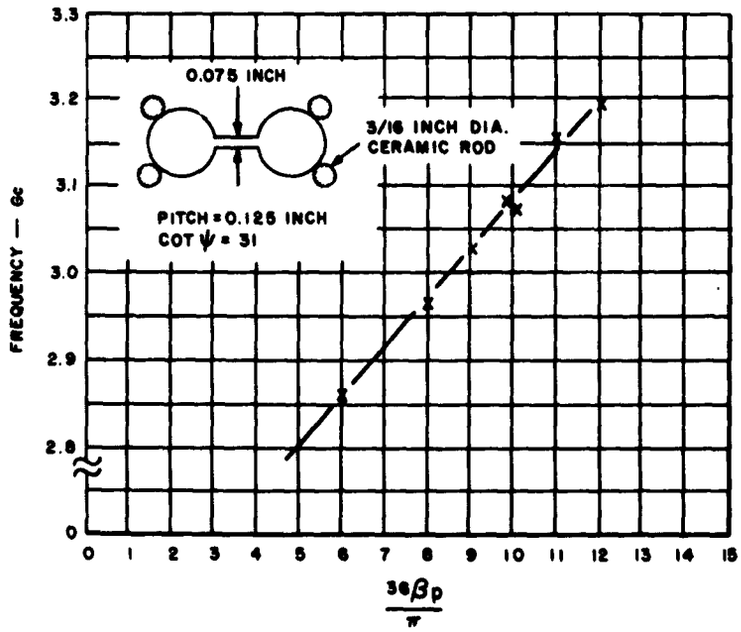

FIGURE 12. ω-β CHARACTERISTICS OF THE MODIFIED BIFILAR HELIX COUPLER - 0.075-INCH SPACING

but reasonably uniform helices have been obtained. The wire used for the helix is molybdenum. The molybdenum is first cold worked and then fired in a furnace to relieve mechanical stress. The support rods have machined grooves for proper spacing of the helix turns. The impedance characteristics are shown in figure 13. The impedance is extremely high, as compared to that of a regular bifilar helix which can be calculated theoretically. The deformation accounts for the high impedance near the axis. Calculations made for the Kompfner-dip length at fixed beam voltage and current showed that the Kompfner dip length was not constant, and modifications must be made to obtain a constant dip length as a function of frequency. The coupler cold loss was also measured; it was lower than the insertion loss of the elliptic helix. The total loss of the coupler at three Gc is about 0.3 db per inch. Therefore, the minimum noise factor for this coupler at S-band is approximately 0.9 db if no coupler cooling is employed. The molybdenum wire was copper plated in the insertion loss measurements. Further loss reduction can be achieved by optimizing the ratio of the wire size to helical pitch.

2-3. KOMPFNER-DIP EXPERIMENT

To investigate the characteristics of the coupler and the beam velocity spread effect, a Kompfner-dip experiment was set up.

Figure 14 shows the experimental apparatus which includes the drift tube, input coupler, output coupler, and collector. The drift tubes, used to form a shielding system for the beam, are placed as close to the coupler as possible without disturbing the r-f matches. Both the electron gun and the collector are electrically insulated from the coupler for beam-current control. The axial magnetic field has been measured accurately; figure 15 shows a plot of the field at the axis of the solenoid. The input and output coupler are placed where the field variation is very small; this is believed to be necessary for minimizing the interchange of different noise powers associated with different modes. The experiment was designed so that the amount of magnetic-field flux threading the cathode could be varied. An experiment was performed to determine the flux distribution in the gun region. The flux lines were not parallel to the electron trajectories, which is a condition for minimum beam interception at the gun anode. For this reason, in subsequent experiments the flux is mostly excluded from the cathode and the interception at the anode is minimized. As shown in figure 14 the apparatus is enclosed in a vacuum bell jar for ease of mounting and demounting, and alteration of components.

Figure 16 illustrates the test setup for measurement of the input coupler characteristics. A similar setup was used to measure the output coupler characteristics. With a signal applied to the input end of the coupler, the decrease in signal level at the output end of the same coupler is recorded as a function of beam voltage, magnetic field, and beam current. The greater the dip, the greater the portion of input signal transferred to the beam wave. The theoretical relationships in the traveling-wave fast-cyclotron-wave coupler which have been verified in this experiment are:

- Synchronization of circuit wave to fast cyclotron wave
- Kompfner dip length
- Passive coupling equation.

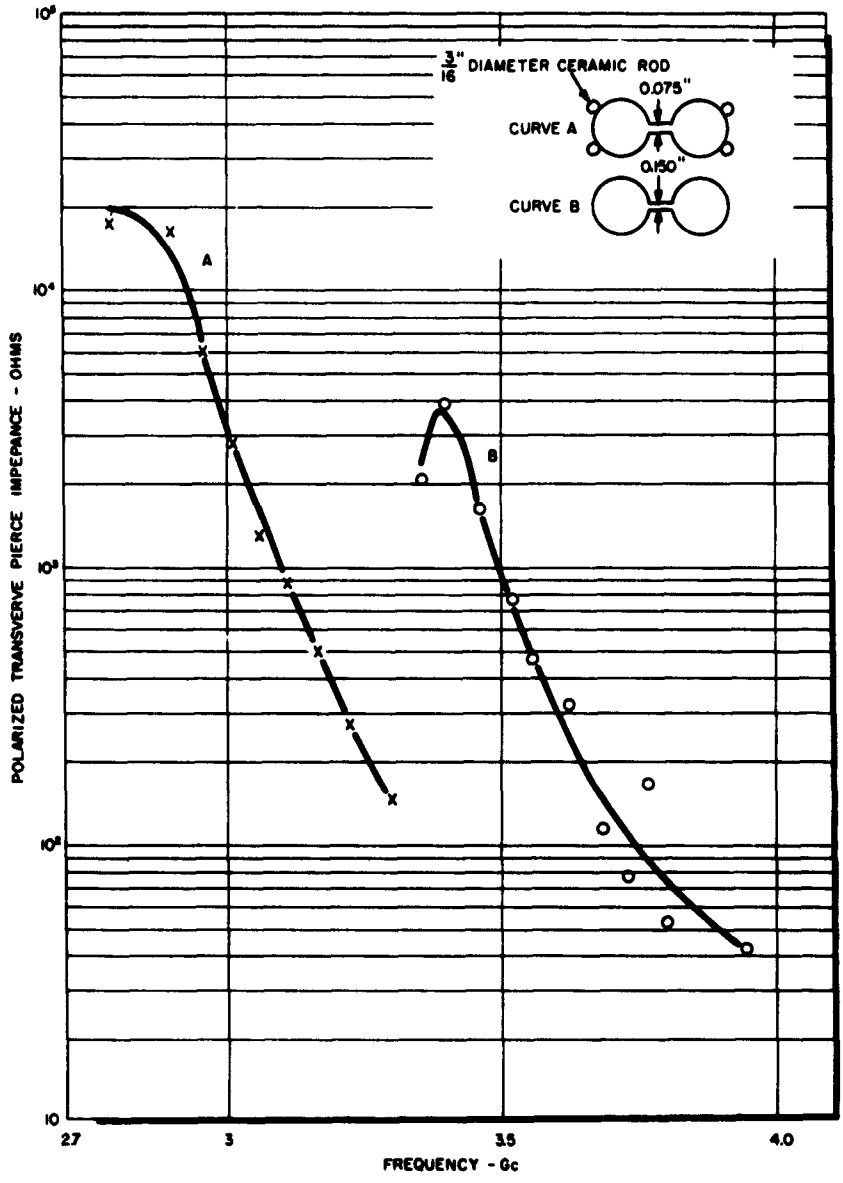

FIGURE 13. TRANSVERSE IMPEDANCE OF MODIFIED BIFILAR HELIX

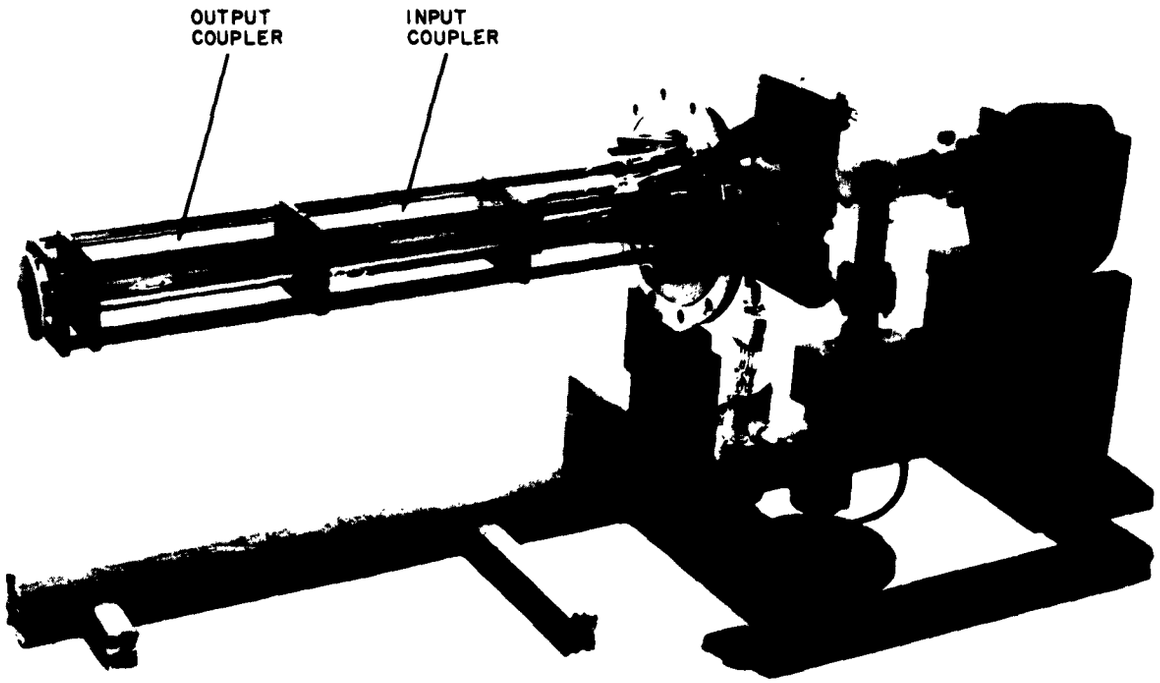

FIGURE 14. KOMPFNER DIP EXPERIMENTAL APPARATUS

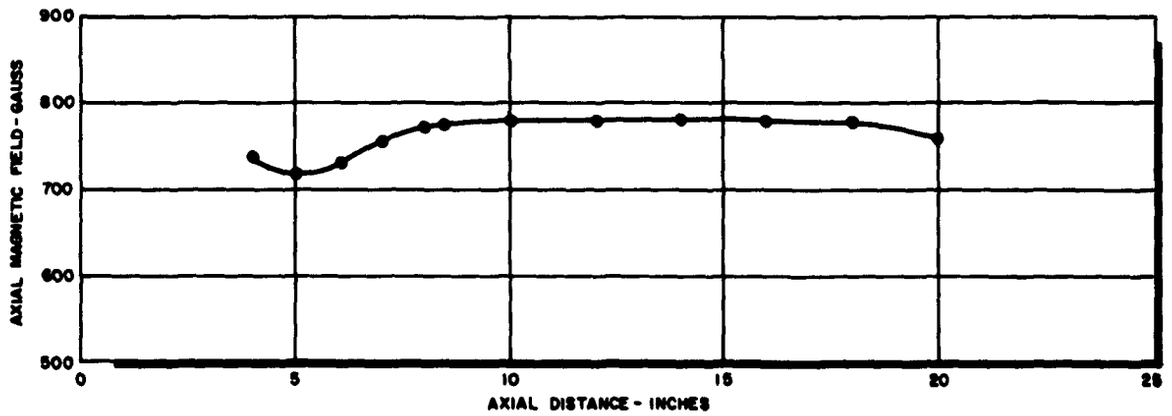

FIGURE 15. AXIAL MAGNETIC FIELD VERSUS DISTANCE

A. Synchronization of Fast Cyclotron Wave

The fast cyclotron wave and the circuit wave must be synchronous for best coupling. In the experiment, the circuit-wave propagation is fixed and is known from cold measurements. The beam-wave propagation is given by $\omega = u_o \beta + \omega_c$, where u_o is the beam velocity and ω_c is the radian cyclotron frequency. Therefore, for a given magnetic field and beam voltage, the propagation characteristic of a fast cyclotron wave is determined. The dip is maximum when the two waves are in synchronization. Figure 17 shows a replot of the circuit $\omega - \beta$ characteristics shown in figure 12. At each frequency, the value of β for the cyclotron wave is calculated with the beam voltage and magnetic field adjusted for maximum dip. The beam propagation characteristics are also shown on figure 17. It can be seen that the two waves are synchronous. A sample calculation of the abscissa of figure 17 as follows:

$\omega = (3100) \times 2\pi \times 10^6$ radians per second

$\omega_c = (2690) \times 2\pi \times 10^6$ radians per second

$u_o = 0.031 \times 3 \times 10^8$ meters per second

$p = 0.125 \times 2.54 \times 10^{-2}$ meter

$$\text{abscissa} = \frac{36\ p\ \beta}{\pi} = \frac{36\ p}{\pi}\left[\frac{\omega - \omega_c}{u_o}\right] = 10.1$$

B. Kompfner Dip Length

The Kompfner dip length is given as

$$L_k = \frac{\lambda_g}{2}\sqrt{\frac{\omega_c}{\omega}\frac{2\ V_o}{I_o\ K_t}} \qquad \text{(see equation 2)}$$

Rearranging the Kompfner dip length equation yields

$$K_t = \frac{1}{2}\left[\frac{\lambda_g}{L_k}\right]^2 \frac{\omega_c\ V_o}{\omega\ I_o}$$

which is equal to 4100 ohms for the following experimental values:

$V_o = 240$ volts

$I_o = 10^{-3}$ ampere

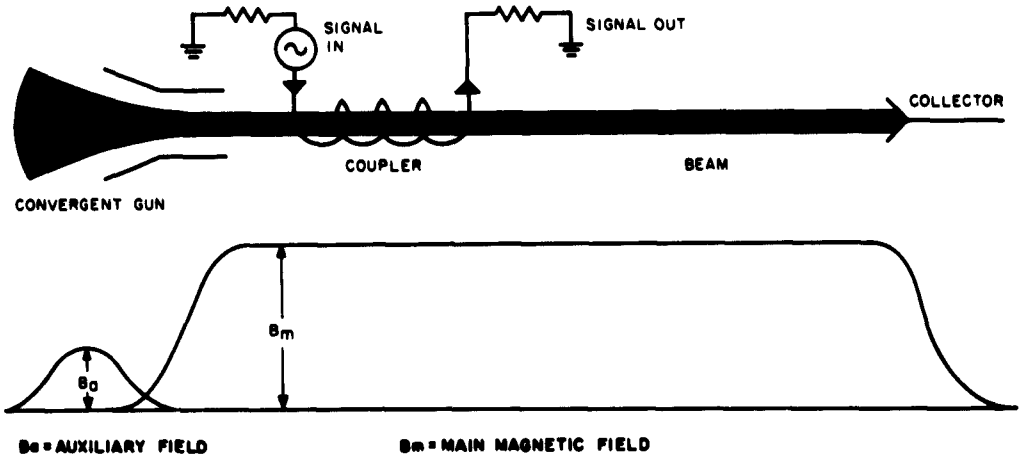

FIGURE 16. KOMPFNER DIP EXPERIMENTAL MEASUREMENT

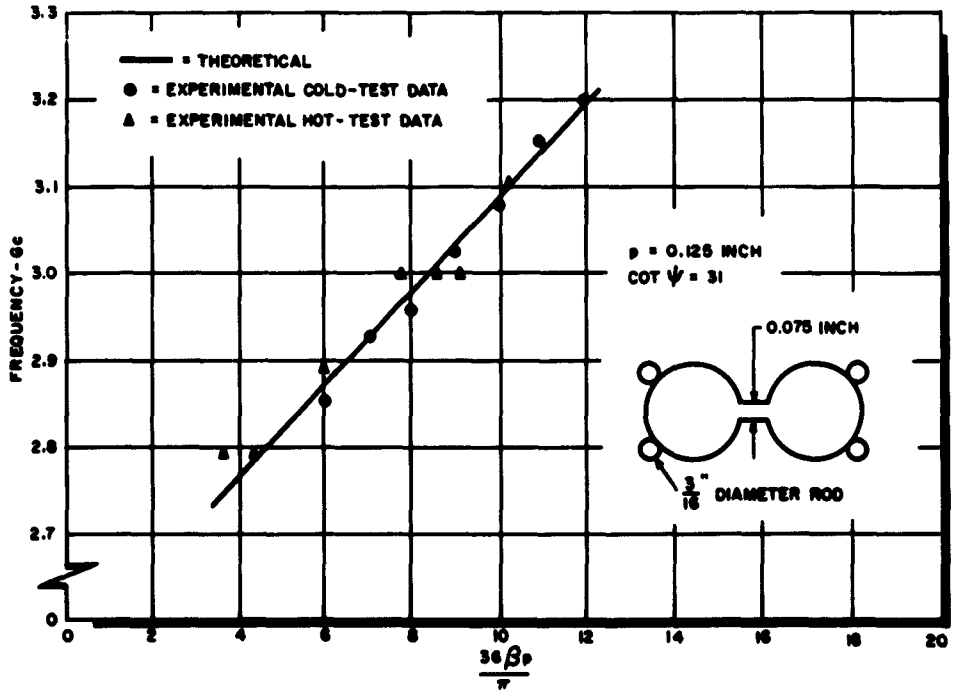

FIGURE 17. ω-β CHARACTERISTICS OF A MODIFIED BIFILAR HELIX

$$f = 2.950\ G_c$$

$$f_c = 2.660\ G_c$$

$$L_k = 6.5 \times 2.54 \times 10^{-2}\ \text{meter}$$

$$\frac{36p\beta}{\pi} = \frac{36p}{\pi}\,\frac{2\pi(2950 - 2660)}{u_o} = 7.1$$

$$\lambda_g = \frac{2\pi}{\beta} = 0.032\ \text{meter}$$

The linearly polarized cold impedance of the circuit is about 7000 ohms. This corresponds to a circularly polarized wave with an impedance of 3500 ohms, which is within the range of experimental error. During the experiment reversal of magnetic field had practically no effect on the dip data; this indicates that the field is linearly polarized.

C. Passive Coupling Equation

To verify the passive coupling theory, a dip versus beam current experiment was conducted. The theoretical Kompfner dip for synchronous operation as a function of beam current has been calculated using the formula

$$\text{Dip} = 10 \log \left[1 - \sin^2 \frac{\pi}{2}\sqrt{\frac{I}{I_b}} \right] \text{db}$$

where I is the beam current and I_b is the beam current corresponding to complete power transfer between circuit and beam. Figure 18 shows both the theoretical curve and the experimental points, which confirm very well the theory of signal transfer. The beam current was adjusted independently of beam voltage by applying different voltages to electrodes located beyond the anode.

The dip versus frequency is plotted in figure 19 for two conditions: (1) perveance held fixed and (2) current adjusted independently for maximum dip. Beam current was varied to compensate for the nonideal impedance characteristics. Early in the experiment, the magnetic field was reversed, and it was found that the dip was practically unchanged. This is believed due to the linearly polarized nature of the transverse electric field. Consequently, all experiments were performed without any magnetic-field reversal. The normal field direction is such that the electrons spiral in the same sense as the bifilar helix.

2-4. SIGNAL ATTENUATION EXPERIMENTS

Signal attenuation caused by the velocity spread was studied using the experimental setup shown in figure 20. At conditions in which the dips are large, the flux linkage to the cathode was varied by changing the auxiliary electromagnetic current. The Kompfner dips were then measured, and the magnitude of the input signal recovered at the output end of the output coupler was measured.

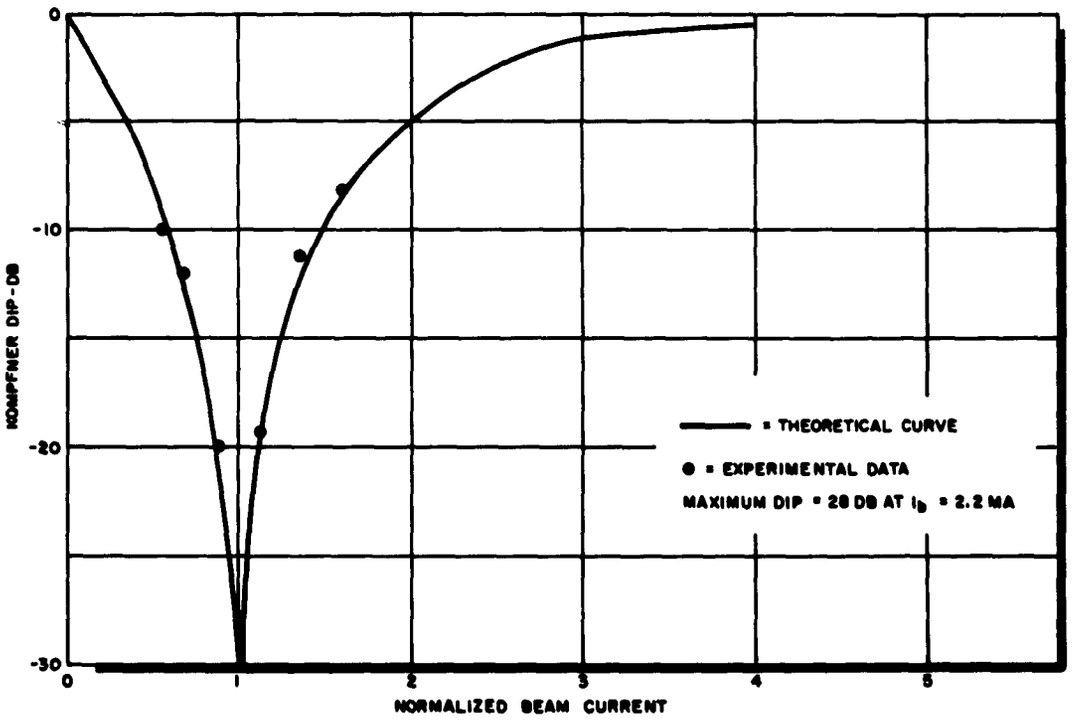

FIGURE 18. KOMPFNER DIP VERSUS NORMALIZED BEAM CURRENT

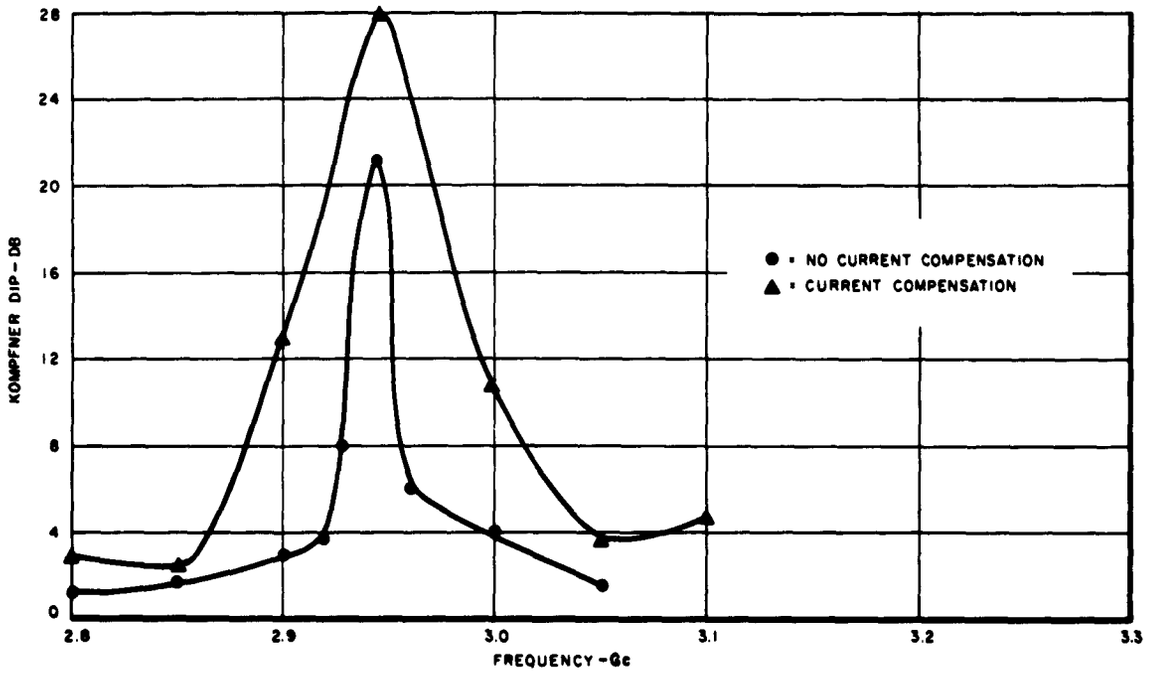

FIGURE 19. KOMPFNER DIP VERSUS FREQUENCY

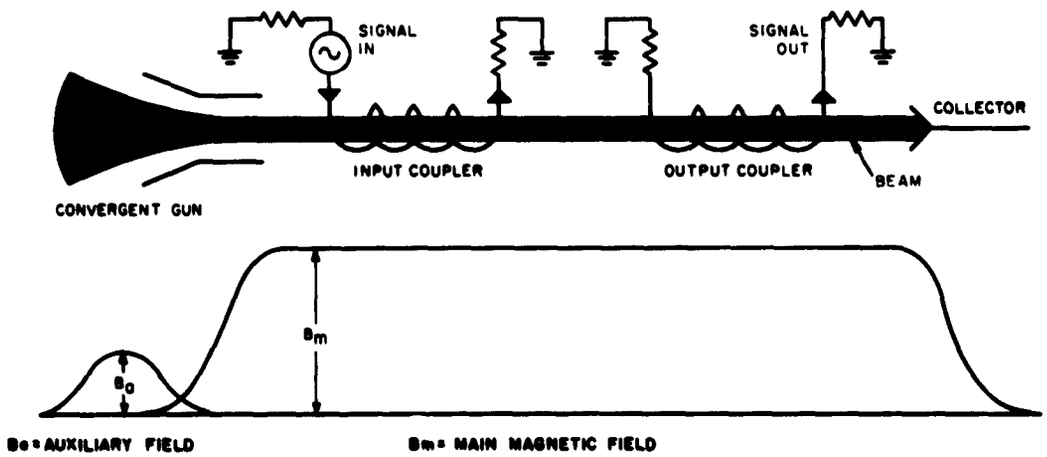

FIGURE 20. VELOCITY SPREAD EXPERIMENTAL APPARATUS

See figure 20. A plot of the percentage cathode flux linkage versus the cathode magnet current which produced a flux aiding the main field in the experiment is shown in figure 21. Because of coaxial-line loss and coupler mismatch, only a rough estimate of the effect of the cathode flux linkage can be made. Figure 22 illustrates the possible signal loss due to velocity spread in the beam. It is noted that the velocity spread effect is quite pronounced as a function of cathode magnetic field. It has also been found that the dip was large at the point of minimum signal loss; this is in agreement with the theory that the power transfer cannot be complete for a multi-velocity beam.

2-5. OSCILLATION

In the early phase of the Kompfner dip measurement, it was found that space-charge-wave oscillation occurred at approximately 350 mc. Different methods were tried to suppress the oscillation, but they were not too effective because of the inaccessibility of the setup in the vacuum bell jar. The oscillation was eliminated by operating at a slightly lower beam voltage. Oscillation frequency as a function of beam voltage was studied. The causes of the oscillation are that the in-phase mode has a rather high value of longitudinal impedance and is not well matched at low frequency. The solution of this problem is to use a good termination at one end of the coupler, as shown in the output end of the input coupler in figure 23. For the output coupler, the same method is to be used. All subsequent measurements were made for a reduced beam voltage so that no oscillation interference could occur.

2-6. COUPLING BETWEEN BIFILAR HELIX COUPLER AND EXTERNAL CIRCUIT, AND COLD CIRCUIT LOSS

The modified bifilar helix supports two modes, only one of which interacts with the fast cyclotron wave. Coupling of the external circuit to the wrong mode will result in a partial loss of the input signal as well as a degradation in the noise quality of the signal; and as long as there is no method of measuring the Kompfner dip other than the one method mentioned in paragraph 2-3, it is very difficult to interpret the dip data if the undesired mode is excited strongly. For these reasons, effort was directed toward attaining a good match between the external circuit and the desired mode. The field configuration of the desired mode is shown in figure 24. The phases of the electric current or fields on the wires are exactly opposite at any given Z-plane (cross-sectional plane). Figure 23 shows a method of connecting the coupler to the external circuit. Cold-test structures were made for the experiment, and the test results are shown in figure 25.

Figure 25 shows that the r-f match is reasonably good, however further improvement can be made, and that the insertion loss per unit length is not negligible. Two methods of measuring the cold circuit loss were used. The traveling wave method is the ordinarily employed insertion loss measurement method. The cavity method requires the determination of the unloaded Q_0 of the circuit, and the loss rate is calculated from the following formula.[3]

$$\text{Loss per wavelength} = \frac{27.3}{Q_0} \frac{v_p}{v_g} \text{ db}$$

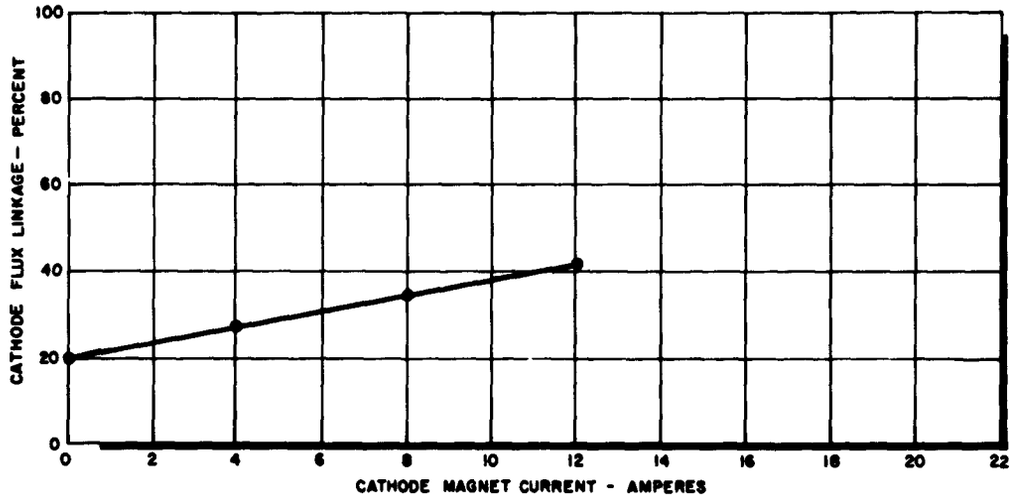

FIGURE 21. CATHODE FLUX LINKAGE VERSUS CATHODE MAGNET CURRENT

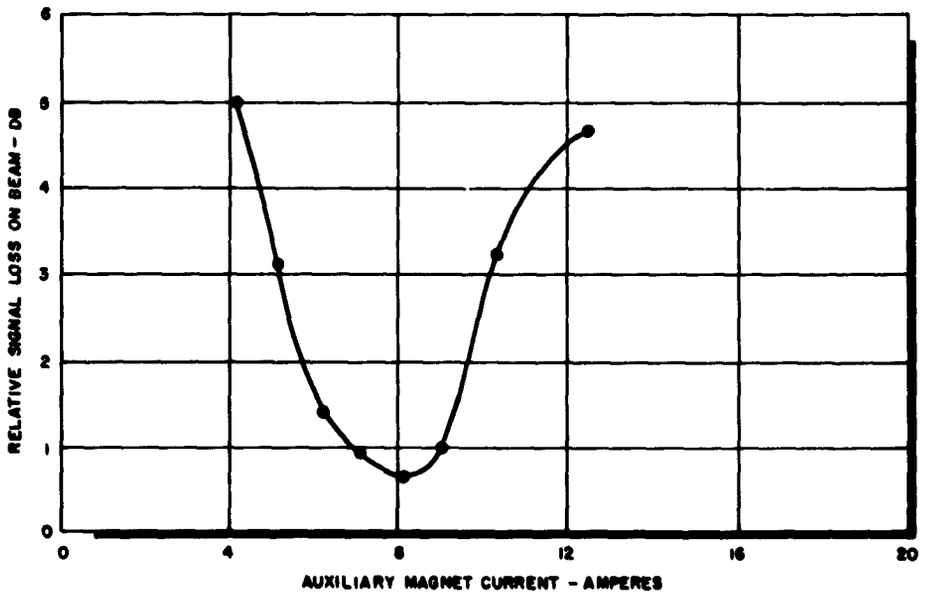

FIGURE 22. SIGNAL LOSS ON BEAM VERSUS AUXILIARY MAGNET CURRENT

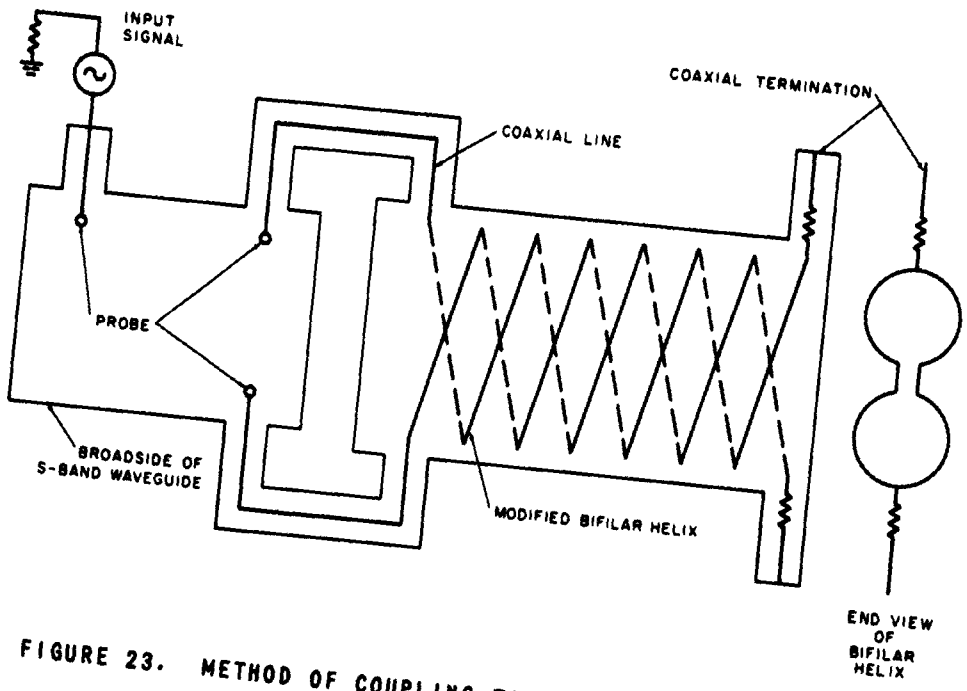

FIGURE 23. METHOD OF COUPLING TO THE ANTI-SYMMETRICAL MODE OF A BIFILAR HELIX

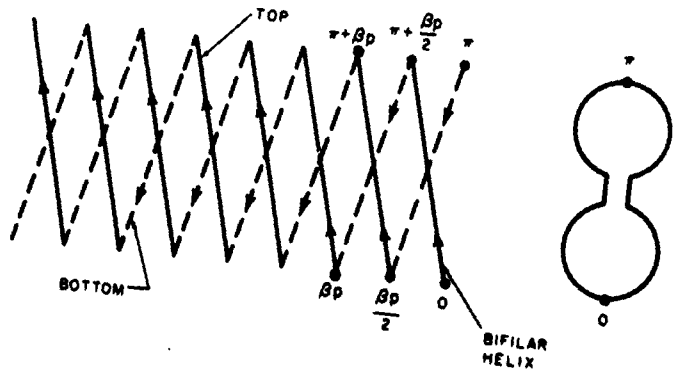

FIGURE 24. CURRENT PHASE OF THE OUT-OF-PHASE MODE OF A BIFILAR HELIX

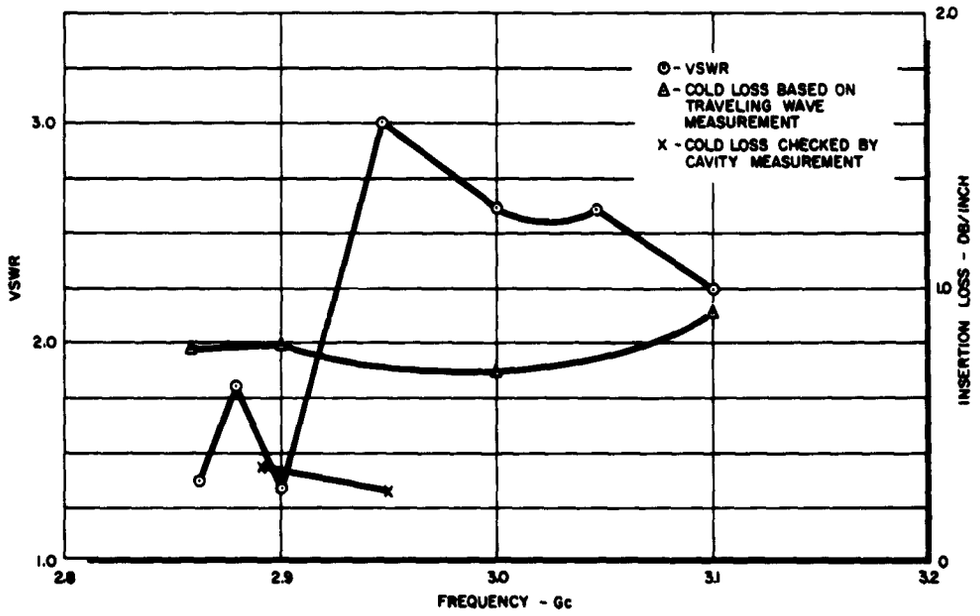

FIGURE 25. VSWR FOR IMPROVED METHOD OF MATCHING AND COLD LOSS RATE OF MODIFIED BIFILAR HELIX

In the cavity measurement, the circuit was not enclosed in a metallic shield whereas in the traveling wave method r-f matching required the use of a shield, which may account for part of the increase in the loss rate. In any case, the lower values of circuit loss rate measured by the cavity method perhaps represent the lower limits of the circuit loss.

2-7. PUMP CIRCUIT

The function of the pump circuit is to amplify the fast cyclotron wave. Three types of pump circuits were studied.

- TE_{11} loaded waveguide
- Four-bar quadrupole circuit
- Quadrifilar helix.

A. TE_{11} Loaded Waveguide

A TE_{11} square waveguide loaded with quadrupolar elements (figure 26) was designed and tested with several modifications. The circuit had sufficient impedance but the impedance value lowered appreciably when the periodicity was increased to that required to yield low values of phase velocity. An excess of electrical energy is stored between elements in the axial direction; and too little is available between elements in a circumferential direction, where the field is desired. Higher space harmonics might yield the desired phase velocity, but, in general, would be very low in impedance. Shaping of the loading elements might increase the field. However, a second more promising, and simpler structure was devised.

B. Four-Bar Quadrupole Circuit

A structure which exhibited the desired low phase velocity, a higher interaction impedance than the TE_{11} loaded waveguide, and manageably low dimensions at 35 Gc is shown in figure 27. The circuit can be described as a TE_{21} loaded circular waveguide with radial slots having an arc length of $r_o\ (\pi/4)$ in the outer wall, where r_o is the outer radius of the circuit. It combines the low phase velocity of an open structure with the high impedance of the loaded waveguide.

The phase velocity measurement indicated that there are two transverse electric modes. The phase velocity characteristics are shown in figure 28 and figure 29. Since the mode separation is very small the possibility exists that the unwanted mode may be coupled to the beam. The field for each of these modes was analyzed by field probing using dielectric beads. The result is shown on figure 30. The faster mode, or Mode B, has impedance which does not increase rapidly with radial distance. The field may not decay to zero at the axis. Therefore, Mode B cannot be used for quadrupole amplification. On the other hand, Mode A has the desired impedance which decreases rapidly as the radial distance decreases. This, in turn, suggests that the field quantity which is proportional to the square root of the impedance may decrease linearly toward the axis, a requirement to be satisfied for low-noise parametric pumping. Figure 31 is a plot

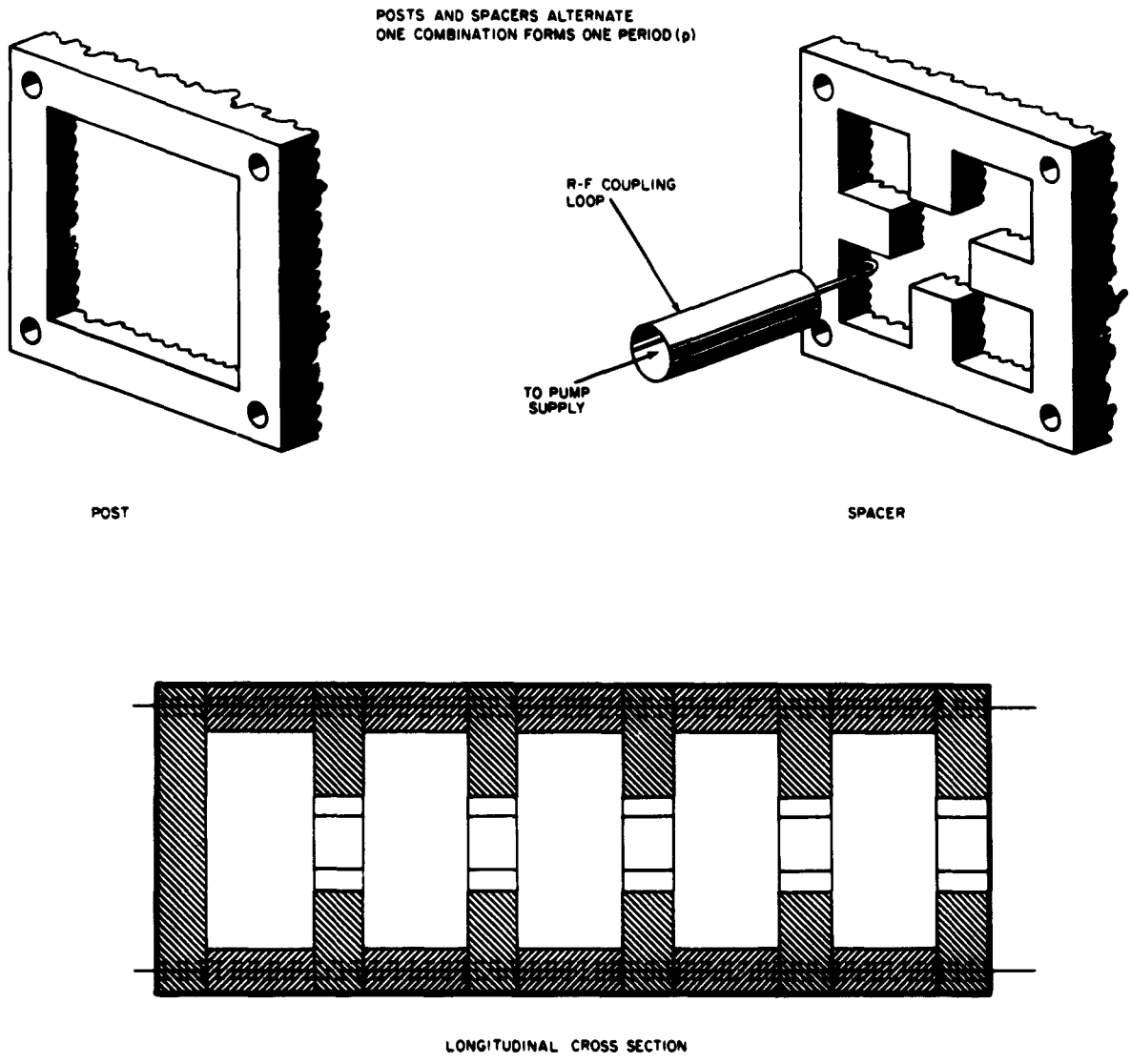

FIGURE 26. TE_{11} SQUARE WAVEGUIDE LOADED WITH QUADRUPOLAR ELEMENTS

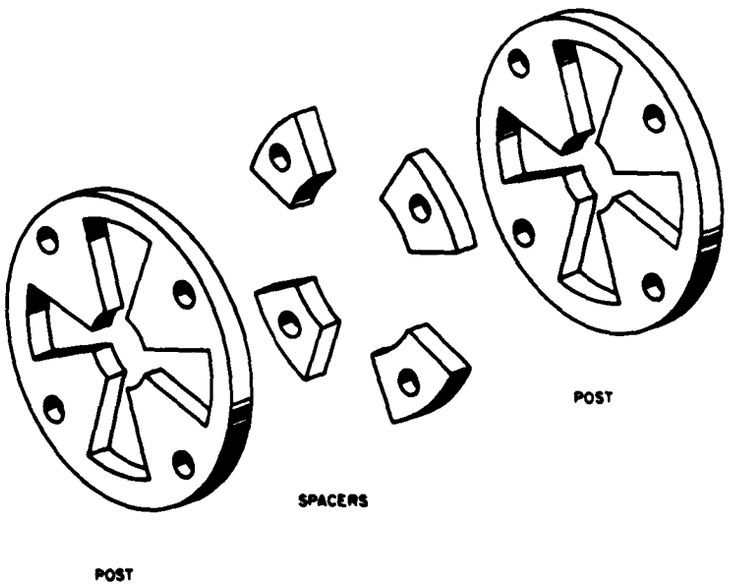

FIGURE 27. FOUR-BAR QUADRUPOLE CIRCUIT

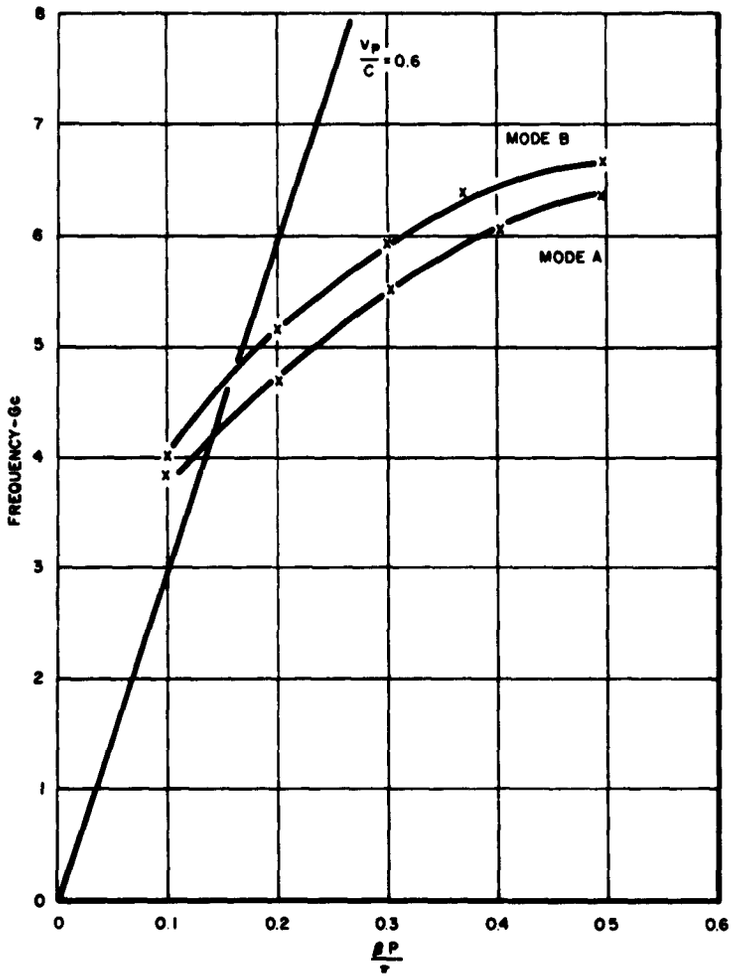

FIGURE 28. ω-β CHARACTERISTICS OF FOUR-BAR QUADRUPOLE CIRCUIT
P = 0.120 INCH

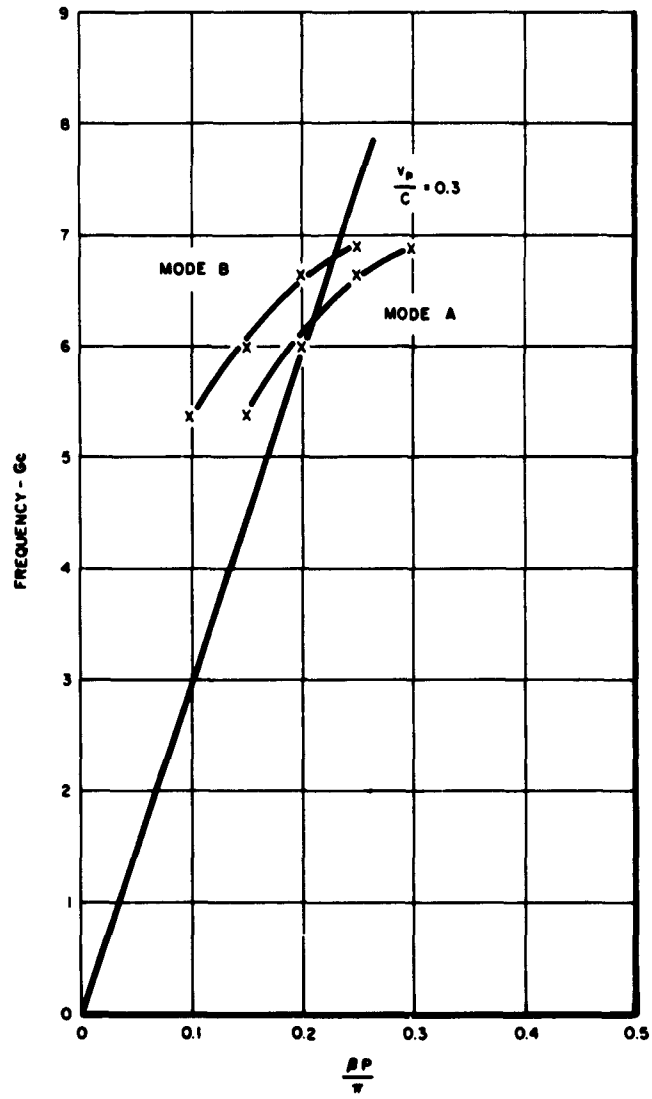

FIGURE 29. ω-β CHARACTERISTICS OF FOUR-BAR QUADRUPOLE CIRCUIT
P = 0.060 INCH

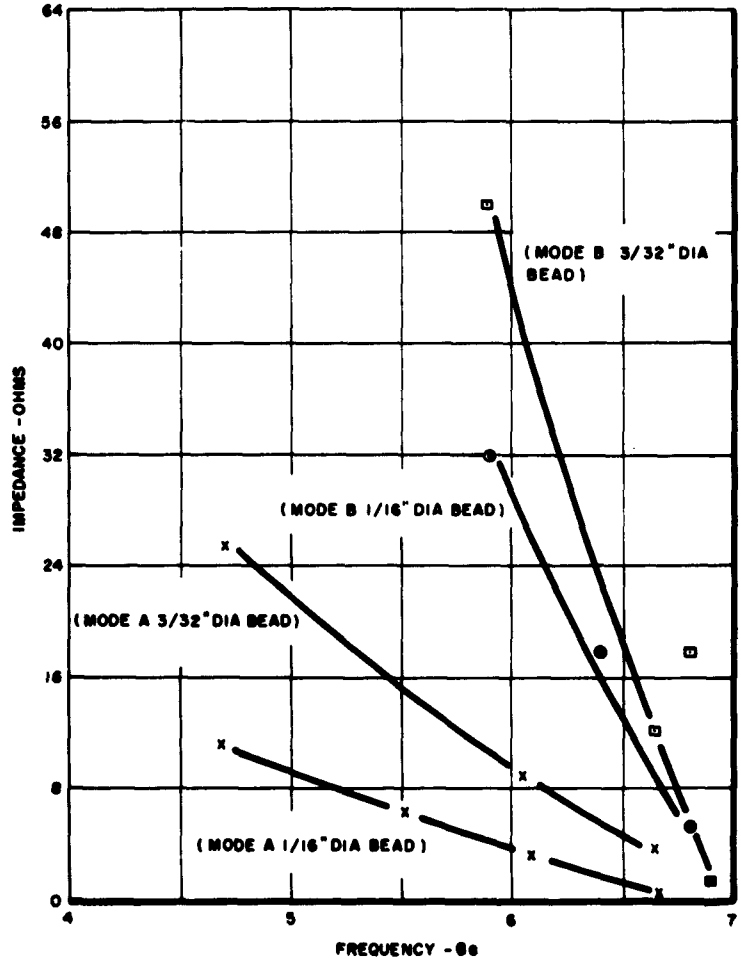

FIGURE 30. IMPEDANCE OF FOUR-BAR QUADRUPOLE CIRCUIT
P = 0.120 INCH

of field pattern at a fixed frequency for Mode A. It indicates the quadrupole nature of the field. The pump is self-supporting and represents no particular construction problem. The parts are stamped out and stacked together to obtain a final thickness of pitch about one-eighth inch. The Q measurement showed that the circuit has a Q greater than 500. A higher value of Q can still be achieved by proper stacking and careful machining of parts.

C. Quadrifilar Helix

The possibility of using the quadrifilar helix as a pump circuit was examined because of the readily available information on the propagation and impedance characteristics of a quadrifilar helix. The experimental setup for the measurement of the pump $\omega - \beta$ characteristic is illustrated in figure 32. A movable probe is used to detect the standing-wave pattern produced by two opposite traveling waves. The resultant $\omega - \beta$ waves for a quadrifilar helix are shown on figure 33 for two cases of dielectric loading. The impedance near the axis of the helix was so low that it was impossible to measure the impedance. A modified quadrifilar helix was made and is shown in figure 34. Experimental data seems to indicate that the impedance near the axis is quite high. The construction of the modified quadrifilar helix is similar to that of the modified bifilar helix. However, accurate reproducibility is much harder to obtain. In addition it was difficult to determine exactly the $\omega - \beta$ curve for the modified quadrifilar helix.

2-8. DEGENERATE DEVICE OPERATION

To simplify the construction problem, it was decided to use the four-bar quadrupole circuit as a pump circuit for parametric amplification. The pump frequency was determined by the coupler requirement. The number of period for the pump circuit was chosen to be 11, so that one of the resonance frequencies is 5800 mc, or approximately twice the signal frequency at degenerate operation. Good r-f match at resonance was achieved by feeding the coaxial line parallel to the pump axis, and through the center of one of the four spokes. The VSWR value at resonance was less than 1.5. The cavity has only one input. A degenerate device consisting of an input coupler, pump, and an output coupler was assembled. The electron gun and collector were of the same design as those in the Kompfner dip experiment.

Figure 35 illustrates the experimental set up for measuring the gain of the degenerate device. Both the signal and pump were modulated by a 1000 cps square wave. This enables measurement of the voltage gain by calibrating the oscilloscope. Figure 36 shows a scope trace of the level of the output signal. The highest level V_2 is the signal level when both the pump and signal are on. The middle level V_1 is the signal level when the pump is off and the signal is on, and the lowest level is the level when the signal is off. The pump field appears to have no effect on the beam when the signal is off. The ratio of the output signal with and without the pump on is the amplitude gain (V_2/V_1). The power gain is proportional to the square of the amplitude ratio. Figure 37 shows a plot of the electronic gain function of signal frequency at a fixed pump power. As stated in paragraph 2-1 of this report, the electronic gain is independent of the signal frequency. The plot of figure 37 is not exactly as predicted. A possible cause is that the coupler field distribution is a function of the signal frequency. At a signal frequency different from one-half the pump frequency, a signal at the idler frequency was observed whenever there was electronic gain.

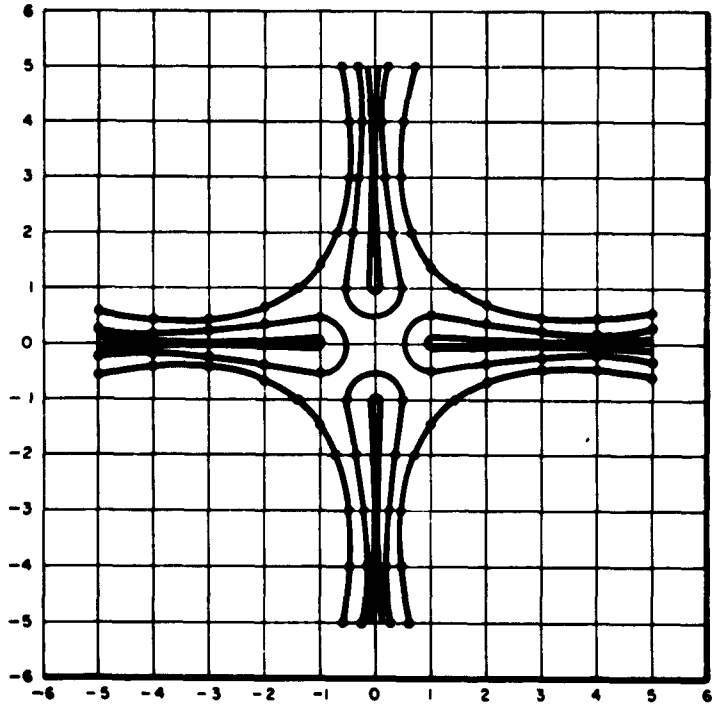

FIGURE 31. FIELD PATTERN HALF-WAY BETWEEN POSTS OF PUMP CIRCUIT AT 4775 MC

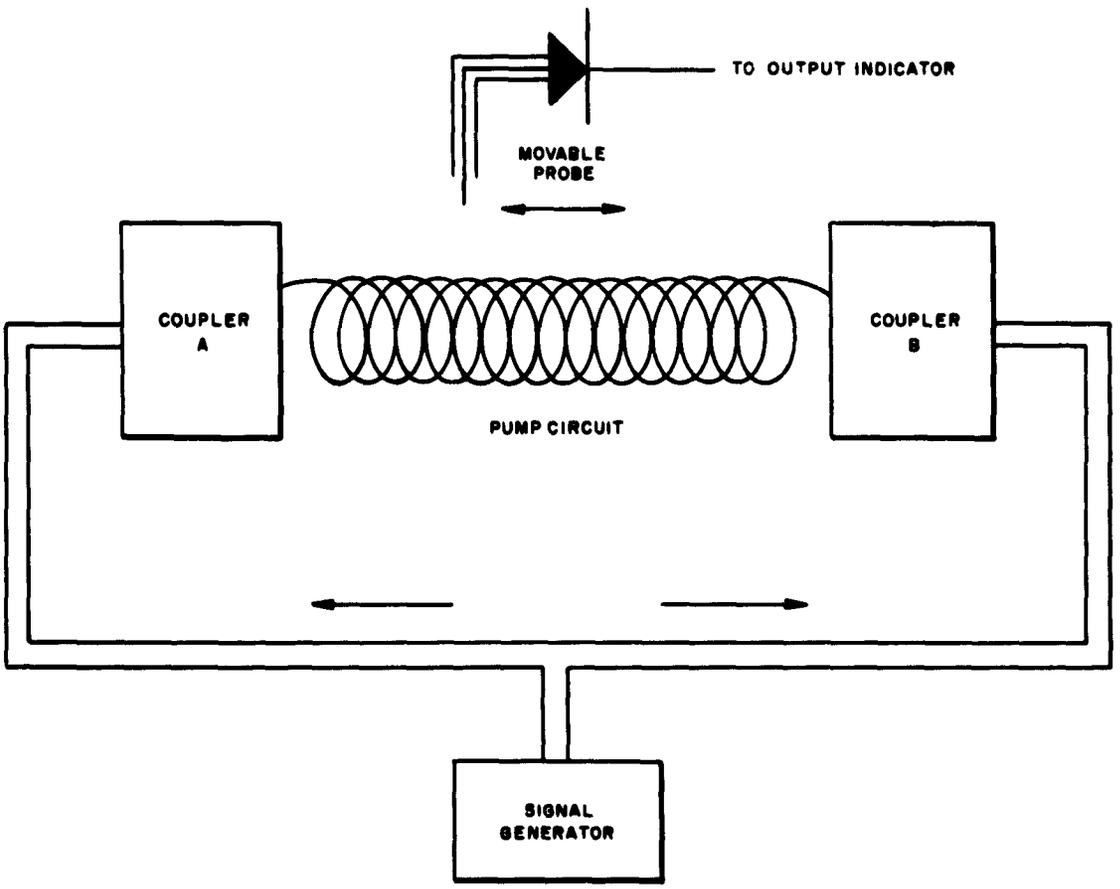

FIGURE 32. ω-β MEASUREMENT EQUIPMENT

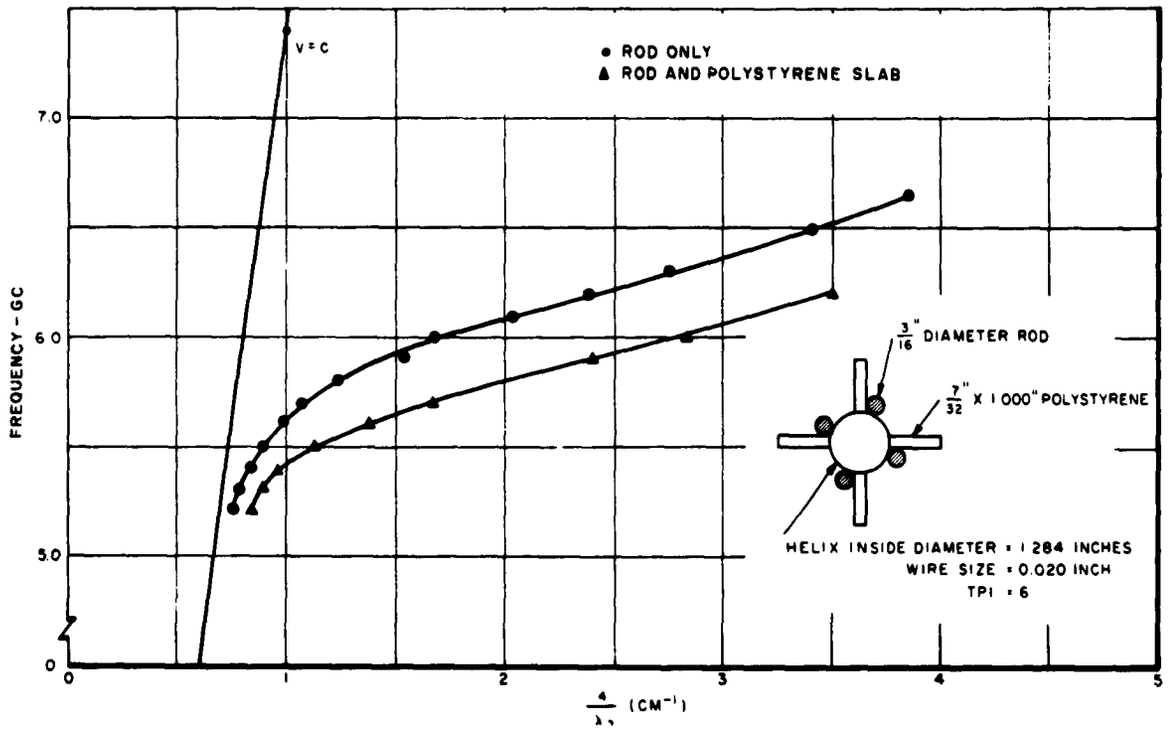

FIGURE 33. ω-β CHARACTERISTICS OF A QUADRIFILAR HELIX

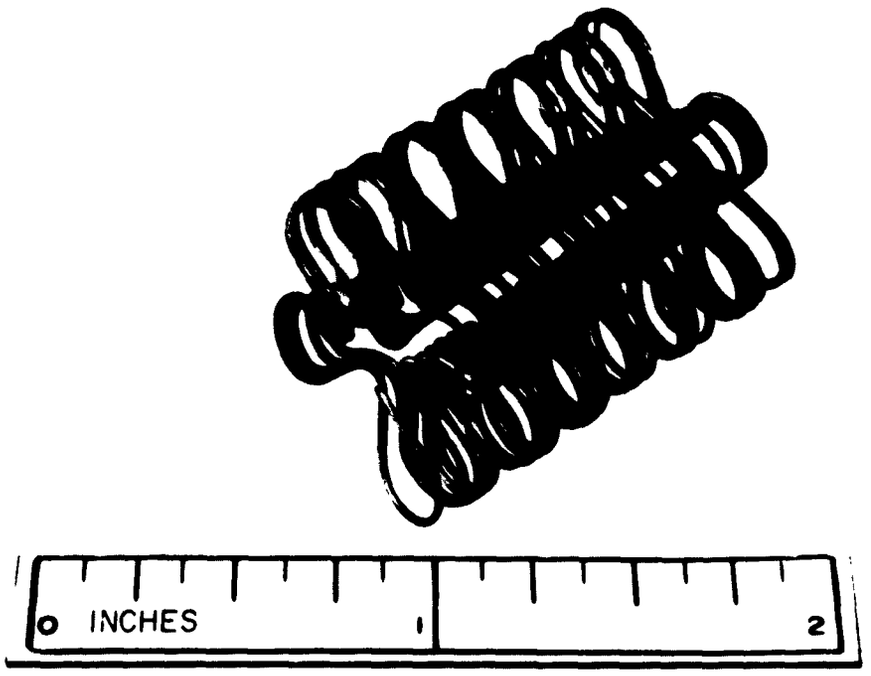

FIGURE 34. MODIFIED QUADRIFILAR HELIX

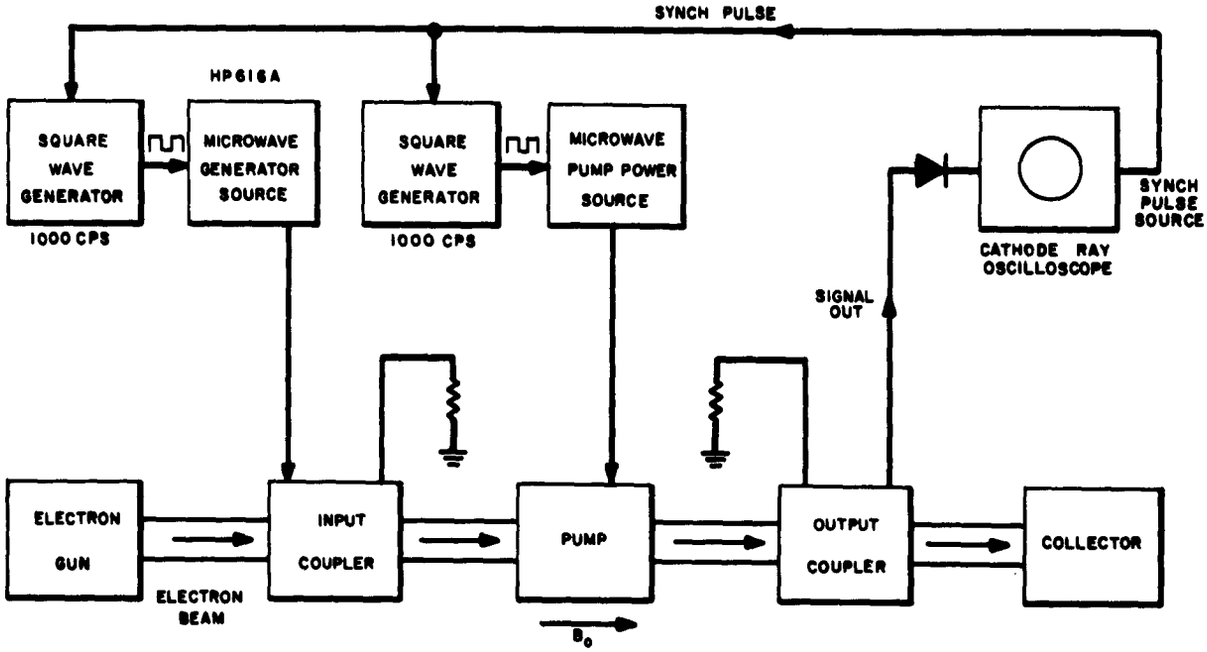

FIGURE 35. EXPERIMENTAL SETUP FOR MEASURING ELECTRONIC GAIN

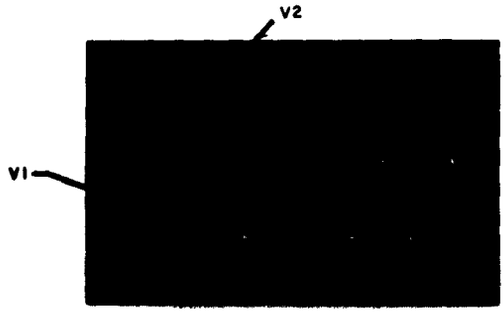

FIGURE 36. SCOPE TRACE OF OUTPUT SIGNAL LEVEL

Figure 38 is a plot of the electronic gain versus pump power. The experimental curve appears to have the opposite curvature at gain values of greater than 10 db. It was noted that electron beam interception occurred even at zero input signal. Orbit pumping is probably present.

Figure 39 shows a plot of gain versus input signal level. The amplification of the device is linear over a broad range of input signal. At lower values of input signal, the presence of a 60 cycle stray signal prevented accurate measurement.

Large external coupling losses plus the coupler distributed loss resulted in a degenerate device that had no net r-f gain from the input terminal to the output terminal. The noise stripped off the input coupler was measured with a noise figure measuring gear which has a noise figure of about 8 db, which was found to be adequate for the application. The stripped noise was found to have a temperature of approximately 30,000°K, or of the same order of magnitude as the product of the convergence of the electron gun and the cathode temperature. The Kompfner dip was not large in the input coupler, and the noise figure measurement showed that the excess noise temperature of the device was also approximately 30,000°K. Because of the highly convergent gun used the order of magnitude of the noise temperature was not unexpected.

2-9. VOLTAGE-TUNED OPERATION

No detailed voltage-tuned operations were studied. Since the Kompfner dip experiment was conducted at a lower voltage than that required for broadband operation, it is essentially a voltage-tuned operation. However, a theoretical study of voltage-tuned operation is discussed.

To facilitate a better explanation of the various modes of operations, the Tien relations for the signal coupler, idler stripper, and pump will be rearranged slightly. These relations are:

$$\omega_s = U_o\beta_s + \omega_c$$

$$\omega_i = U_o\beta_i + \omega_c$$

$$\frac{\omega_p}{2} = U_o\frac{\beta_p}{2} + \omega_c$$

$$\frac{\omega_s + \omega_i}{2} = \frac{\omega_p}{2}$$

$$\frac{\beta_s + \beta_i}{2} = \frac{\beta_p}{2}$$

These relationships show that the points (ω_s,β_s), (ω_i,β_i), and $(\omega_p/2)$, $(\beta_p/2)$ are colinear for a given magnetic field and a given beam velocity. The point $(\omega_p/2,\beta_p/2)$ is called the pump half-point and will be used throughout the following discussion. It lies exactly half-way between (ω_s,β_s) and (ω_i,β_i).

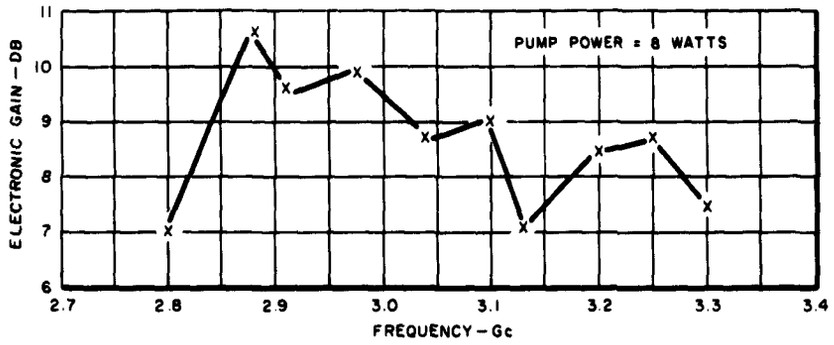

FIGURE 37. ELECTRONIC GAIN VERSUS FREQUENCY

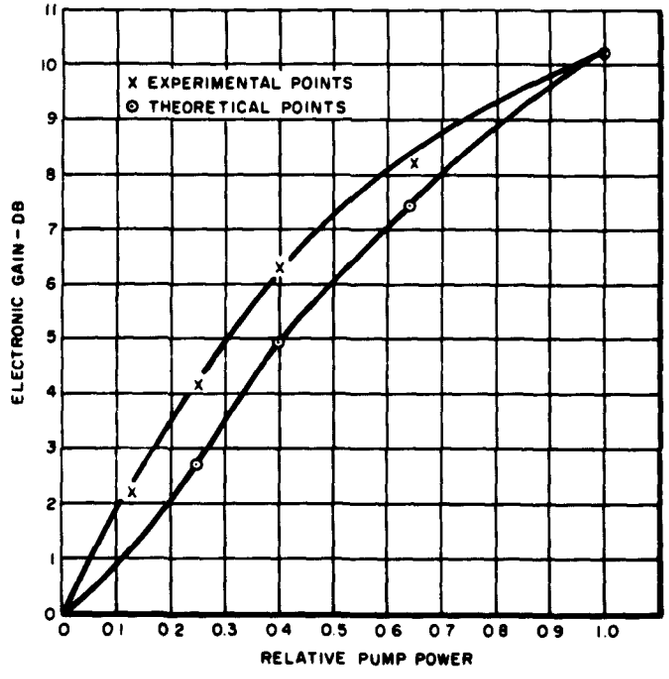

FIGURE 38. ELECTRONIC GAIN VERSUS PUMP POWER

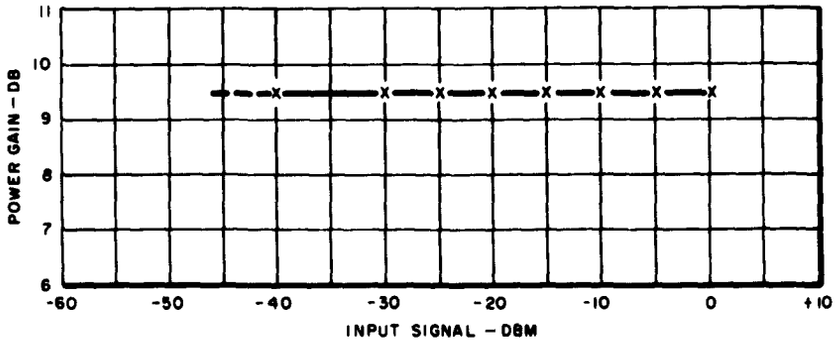

FIGURE 39. ELECTRONIC GAIN VERSUS INPUT SIGNAL

Figures 40 through 43 illustrate the four possible types of operation; namely,

- Fixed pump point, variable uniform beam voltage and variable uniform magnetic field
- Fixed uniform magnetic field, variable pump point and variable beam voltage
- Fixed pump point, fixed uniform magnetic field and variable coupler voltage
- Fixed pump point, fixed uniform beam voltage and variable coupler magnetic field.

Figures 40 and 41 illustrate two possible methods of tuning in which both the beam voltage and magnetic field are uniform throughout the length of the tube. In figure 40, the pump half-point is fixed, and the magnetic field and the beam voltage are tuned simultaneously. The signal coupler tuning curve and the idler stripper tuning curve are rotationally symmetrical about the pump half point. This method's main disadvantage is that the tuning rate is limited by the coil inductance of the electromagnet. Its advantages are that the bandwidth of the idler circuit is more narrow than that of the signal coupler, and the gain at the pump circuit is somewhat insensitive to beam voltage or signal frequency. Figure 41 illustrates the operation when the pump point is tuned with the beam voltage while the magnetic field is fixed. The restriction imposed in the first case is removed. However, the bandwidth for the idler is greater than that of the pump which, in turn, is greater than that of the signal coupler. One disadvantage is that the bandwidth is limited by the pump circuit bandwidth.

Figures 42 and 43 illustrate the cases in which either the magnetic field, the beam voltage, or both, are tuned in the coupler region with respect to the rest of the device. The principle of operation is as follows: First, by tuning the beam voltage or magnetic field, the fast cyclotron wave at the signal frequency is excited in the beam as a result of coupling. Second, when this signal travels to a different electric potential or magnetic field region, the wave length or phase shift β is transposed to a different value lying exactly on the idler line required by the Tien relations. The signal is amplified and coupled out just as in the broadband case. The main advantage of this method of tuning is that with the exception of the signal coupler, all other components can be the same as those in the broadband device. However, any change in the beam voltage or magnetic field will couple synchronous noise to the fast cyclotron wave. The mechanism and the degree of this coupling is not well understood, at this time. To overcome this difficulty, it is planned to tune the output coupler so that the signal is amplified before it is coupled to the synchronous mode if synchronous mode coupling is unavoidable.

2-10. AN X-BAND DESIGN OF A FIXED-TUNED BROADBAND DEGENERATE DEVICE

Based on S-band broadband-untuned operation, an X-band version of the device meeting the following specifications is considered to be feasible.

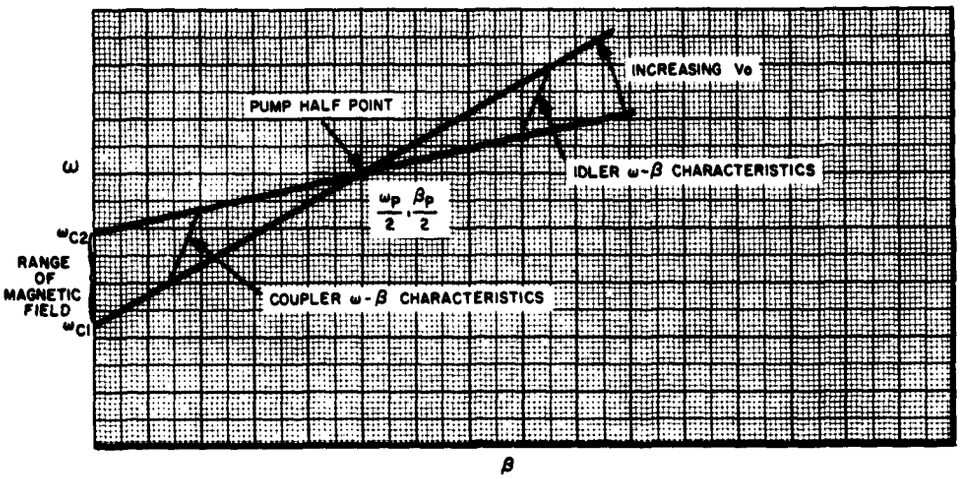

FIGURE 40. FIXED PUMP POINT, VARIABLE UNIFORM MAGNETIC FIELD AND VARIABLE UNIFORM BEAM VOLTAGE OPERATION

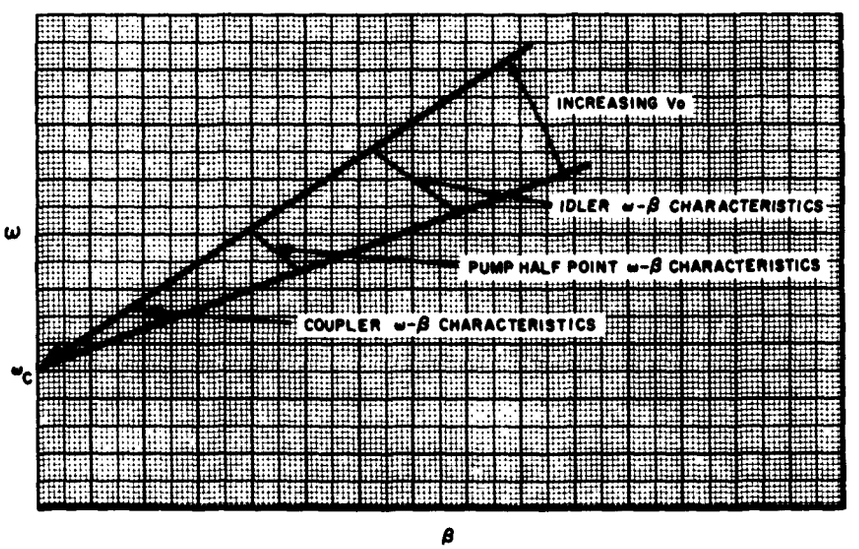

FIGURE 41. FIXED UNIFORM MAGNETIC FIELD, VARIABLE PUMP POINT AND VARIABLE UNIFORM BEAM VOLTAGE OPERATION

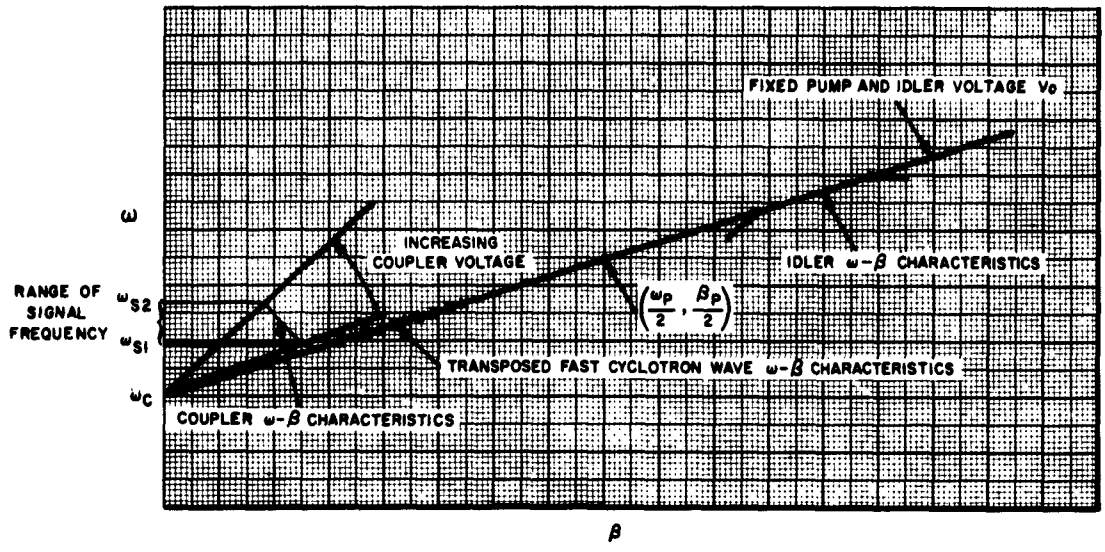

FIGURE 42. FIXED PUMP POINT, FIXED UNIFORM MAGNETIC FIELD AND VARIABLE COUPLER VOLTAGE OPERATION

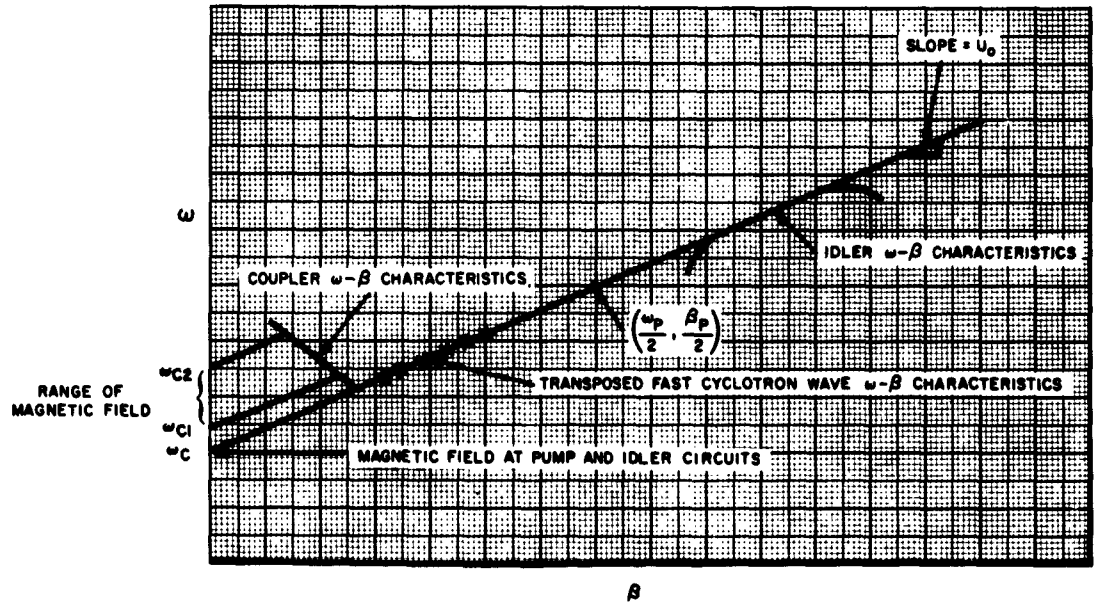

FIGURE 43. FIXED PUMP POINT, FIXED UNIFORM BEAM VOLTAGE AND VARIABLE COUPLER MAGNETIC FIELD OPERATION

Frequency	9.0 to 11.0 Gc
Gain	25 db
Noise Figure	2 db (double channel)
Pump Frequency	20 Gc
Pump Power	10 watts
Beam Voltage	400 volts
Beam Current	16 ma
Magnetic Field	2800 Gauss
Tube Length	9 inches

Other information of interest include:

Beam Diameter	0.009 inch
Cathode Current Density	2 amperes/cm^2
Gun Convergence	20
Coupler Length	3 inches
Pump Length	2 inches
Beam Microperveance	2
Magnetic Inside Diameter	1 inch

In this design, the bandwidth is approximately 20 percent for a circuit group velocity corresponding to 400 volts. The limit on the bandwidth of the coupler depends greatly on the group velocity of the circuit. At low group velocity a small change in frequency can result in a very large change in the propagation constant which, in turn, results in a very large change in the value of the transverse impedance. Experimental data have shown that the change in transverse impedance is too drastic, and a 20 percent bandwidth is about the maximum practical value that can be obtained with a beam velocity corresponding to 400 volts. At twice the circuit group velocity or beam velocity, the bandwidth can be expected to be twice as large or 40 percent. To determine the physical length of the device, the coupler may be considered first. There was no attempt to change the group velocity of the coupler circuit in this program, and the circuit impedance at twice the present group velocity is not known. But, assuming the impedance and the beam current are the same, the coupler will be nearly twice as long or nearly six-inches at X-band.

This seems to indicate that coupler length may be traded for bandwidth in applications in which the latter is warranted. For the pump, the pump length for the present circuit will have to be multiplied by a factor of four in order to provide the same gain. However, it is believed that new pump circuits with much higher values of impedance and Q can be developed to offset the effect of the increase in beam velocity in r-f gain.

SECTION III

CONCLUSIONS

Theoretical studies show that for broadband operations the following requirements must be satisfied for a coupler circuit:

(1) The coupler circuit phase velocity must be finite

(2) The coupler circuit group velocity must be constant for untuned broadband operation

(3) The Kompfner-dip length must be constant for either voltage-tuned or untuned broadband operation.

Cold test data show that the modified bifilar helix has the first two qualities. The third requirement is not present but can still be satisfied by carefully varying the circuit parameters.

For low-noise operations, conditions that must be satisfied by the circuit and the electron beam are:

(1) The circuit must have a high and uniform transverse impedance in the beam region

(2) The total loss of the coupler circuit must be small

(3) The beam voltage must be at least a few hundred volts to minimize the thermal velocity effects

(4) The velocity spread effects must be small.

The modified bifilar helix has been found to have a very high impedance (1), and calculations show that condition (4) is also satisfied. The group velocity of the helix has been formed to correspond to about 400 volts of beam voltage, and condition (3) is met. The total cold loss of the helix, however, is not negligible. The cold loss has been found to be about 4 to 5 db. However, by operating at a higher beam current, the length and thus the loss of the coupler can be made smaller. In addition, the effect of the coupler loss on the noise figure of the device can be reduced by cooling the coupler circuit. Considering all the items mentioned, it can be concluded that the modified bifilar helix represents a very good choice for the application.

To confirm the cold test data, a Kompfner dip experiment was performed. This experiment confirmed the cold test data on the coupler circuit, and good circuit-to-beam coupling was verified by a 28 db Kompfner dip. The experimental bandwidth of the coupler was narrow but was mainly caused by wrong external

coupling, and non-ideal impedance versus frequency variation. From the same experiment, it was found that the velocity spread effect was not large, and that beam noise stripping by the input coupler as a function of cathode flux linkage was optimum at partially immersed flow rather than at fully immersed flow. This points to the need for further study. In addition, a convergent gun was used in the experiment. The gun convergence amplifies the transverse noise by a factor of the order of the area convergence ratio. However, because of the convergence the current density requirement at the cathode is less severe; and this may very well be an advantage at high frequency.

In addition to studying different coupler circuits, several pump circuits were studied. The final choice for the pump circuit is the four-bar quadrupole circuit because it is easier to construct, and it has a potentially higher value of circuit Q. The mode of operation was naturally the resonant mode by taking advantage of the high Q value of the circuit. The electronic gain was nearly independent of signal frequency. The dynamic range of the device appears quite large. Because of circuit loss and coupling loss, no r-f net gain was observed. Experimentally, the electronic gain versus pump power of the device agreed quite well with theory except at higher values of gain. High gain was accompanied by an increase in beam interception, which might be contributed to orbit pumping. Further study in this area is needed.

Finally, some of the problems that have not been fully solved and tested include good broadband r-f matching of the external circuit to the transverse mode of coupler, and at the same time a good transition of the longitudinal mode so that low frequency oscillation cannot occur.

SECTION IV

RECOMMENDATIONS

The modified bifilar helix has been found to offer the best solution for minimizing the velocity spread effects. This helix is also capable of reasonable broadband operation provided a slight modification of the circuit impedance variation with frequency is made. Further work in this area is especially recommended. Because the operating ka values are relatively high for this circuit the circuit loss is not negligible, and detailed means of minimizing this loss have not to date been investigated.

The possibility of using a convergent-flow electron gun as a means of overcoming the difficulty associated with the cathode current density limit is recommended.

The pump circuit can be made more efficient by decreasing the size of the beam hole, and represents a good interaction pump even at high frequency. Further work to increase the impedance is highly desirable.

Further work, both theoretical and experimental, on partially immersed flow gun is recommended since experimental data show that the beam noise stripping appears to be optimum at partially immersed flow.

REFERENCES

1. E.I. Gordon, "Private Communication"

2. C.C. Wang, "Electron Beams in Auxially Symmetrical Electrical and Magnetic Fields" Proc. IRE, Vol. 38, pp. 135-147, February 1950

3. J.R. Pierce, Traveling-Wave Tubes, New York, D. VanNorstand Co., Inc., 1950

BIBLIOGRAPHY

1. R. Adler, "The Quadrupole Amplifier," Proc. IRE, October 1959.

2. Tore Wessel-Berg, Microwave Laboratory Report No. 376, A General Theory of Klystrons with Arbitrary, Extended Interaction Fields, Stanford University, March 1957.

3. S. Sensiper, "Electromagnetic Waves Propagation on a Helical Conductor," M.I.T., Research Laboratory for Electronic Report, May 1953.

4. S. Bloom, "Effect of Distributed-Loss Noise Generators on Traveling-Wave Tube Noise Factors," RCA Review, Vol. 22, p. 347, June 1961.

5. J.R. Pierce and P.K. Tien, "Coupling Modes in Helices," Proc. IRE, Vol. 42, pp. 1389-1396, September 1954.

6. D.A. Watkins, Topics in Electromagnetic Theory, New York, John Wiley, 1958, Chapter 3.

7. S.J. Mason, "Further Properties of Signal Flow Graphs," Proc. IRE, Vol. 44, pp. 920-926, July 1956.

8. Stanford Goldman, Transformation Calculus and Electrical Transients, New York, Prentice Hall, 1950.

9. W.H. Louisell, Coupled Mode and Parametric Electronics, New York, John Wiley, 1960.

DISTRIBUTION LIST

	No of Copies
RAWED, Attn. H. Friedman Rome Air Development Center Griffiss Air Force Base, New York	2
RAAPT Rome Air Development Center Griffiss Air Force Base, New York	1
RAALD Rome Air Development Center Griffis Air Force Base, New York	1
ROZMCAT GEEIA Griffiss Air Force Base, New York	1
Signal Corps Liaison Officer RADC (RAOL, Attn. Maj Norton) Griffiss Air Force Base, New York	1
AUL (3T) Maxwell Air Force Base, Alabama	1
ASD(ASAPRD) Wright-Patterson Air Force Base, Ohio	1
Chief, Naval Research Laboratory AHn: Code 2027 Washington 25, D.C.	1
Air Force Field Representative Naval Research Laboratory Attn: Code 1010 Washington 25, D.C.	1
Commanding Officer USASRDL Attn: SIGRA/SL-ADI Fort Monmouth, New Jersey	1
National Aeronautics and Space Administration Langley Research Center Langley Station Hampton, Virginia Attn: Librarian	1

DISTRIBUTION LIST (Cont)

	No of Copies
Zenith Radio Corporation Attn: Dr. R. Adler Chicago, Illinois	1
Space Technology Laboratories Attn: Dr. I. Kaufaman P.O. Box 1085 Canoga Park, California	1
Stanford Research Institute Attn: Dr. C.W. Barnes Menlo Park, California	1
SFD Laboratories Attn: Dr. J. Saloon 800 Rahway Avenue Union, New Jersey	1
USASRDL Electronic Tube Division, Microwave Tube Branch Attn: Mr. John Carter, SIGRA/FL-PRM Fort Monmouth, New Jersey	1

DISTRIBUTION LIST (Cont)

	No of Copies
Central Intelligence Agency Attn: OCR Mail Room 2430 E. Street NW Washington 25, D.C.	1
Air Force Systems Command (SCSE) Andrews Air Force Base Washington 25, D.C.	1
Command General U.S. Army Electronic Proving Ground Attn: Technical Documents Library Fort Huachuca, Arizona	1
ASTIA (TISIA-2) Arlington Hall Station Arlington 12, Virginia	10
Air Force Systems Command (SCFRE) Andrews Air Force Base Washington 25, D.C.	1
Headquarters USAF (AFOCA) Washington 25, D.C.	1
AFOSR (SRAS/Dr. G.R. Eber) Holloman Air Force Base, New Mexico	1
Office of Chief of Naval Operations (Op-724) Navy Department Washington 25, D.C.	1
Commander U.S. Naval Development Center (NADC Library) Johnsville, Pennsylvania	1
Commander Naval Missile Center Technical Library (Code No. 3022) Point Mugu, California	1
Bureau of Naval Weapons Main Navy Building Washington 25, D.C. Attn: Technical Librarian, DL1-3	1

DISTRIBUTION LIST (Cont)

	No of Copies
Commandant Armed Forces Staff College (Library) Norfolk 11, Virginia	1
ADC (ADOAC-DL) Ent Air Force Base, Colorado	1
AFFTC (FTOOT) Edwards Air Force Base, California	1
Commander U.S. Naval Ordnance Laboratory (Technical Library) White Oak, Silver Spring, Maryland	1
Commanding General White Sands Missile Range New Mexico Attn: Technical Library	1
Director U.S. Army Engineer Research and Development Laboratories Technical Documents Center Fort Belvoir, Virginia	1
ESD (ESAT) L.G. Hanscom Field Bedford, Massachusetts	1
Commanding Officer and Director U.S. Naval Electronics Laboratory (Library) San Diego 52, California	1
ESD (ESAT) L.G. Hanscom Field Bedford, Massachsetts	1
Commandant U.S. Army War College (Library) Carlisle Barracks, Pennslyvania	1
APGC (PGAPI) Eglin Air Force Base, Florida	1
AFSWC (SWOI) Kirtland Air Force Base, New Mexico	1
AFWTC (Technical Library) MU-135 Patrick Air Force Base, Florida	1